Noisy Lagrangian Tracers for Filtering Random Rotating Compressible Flows

Nan Chen, Andrew J Majda and Xin T Tong

Department of Mathematics, and Center for Atmosphere Ocean Science, Courant Institute of Mathematical Sciences, New York University, 251 Mercer Street, New York, NY 10012, USA
chennan@cims.nyu.edu, jonjon@cims.nyu.edu, tong@cims.nyu.edu

October 21, 2014

Abstract

The recovery of a random turbulent velocity field using Lagrangian tracers that move with the fluid flow is a practically important problem. This paper studies the filtering skill of L noisy Lagrangian tracers in recovering random rotating compressible flows that are a linear combination of random incompressible geostrophically balanced (GB) flow and random rotating compressible gravity waves. The idealized random fields are defined through forced damped random amplitudes of Fourier eigenmodes of the rotating shallow water equations with the rotation rate measured by the Rossby number ε. In many realistic geophysical flows, there is fast rotation so ε satisfies $\varepsilon \ll 1$ and the random rotating shallow water equations become a slow-fast system where often the primary practical objective is the recovery of the GB component from the Lagrangian tracer observations. Unfortunately, the L-noisy Lagrangian tracer observations are highly nonlinear and mix the slow GB modes and the fast gravity modes. Despite this inherent nonlinearity, it is shown here that there are closed analytical formulas for the optimal filter for recovering these random rotating compressible flows for any ε involving Ricatti equations with random coefficients. The performance of the optimal filter is compared and contrasted through mathematical theorems and concise numerical experiments with the performance of the optimal filter for the incompressible GB random flow with L noisy Lagrangian tracers involving only the GB part of the flow. In addition, a sub-optimal filter is defined for recovering the GB flow alone through observing the L noisy random compressible Lagrangian trajectories, so the effect of the gravity wave dynamics is unresolved but effects the tracer observations. Rigorous theorems proved below through suitable stochastic fast-wave averaging techniques and explicit formulas rigorously demonstrate that all these filters have comparable skill in recovering the slow GB flow in the limit $\varepsilon \to 0$ for any bounded time interval. Concise numerical experiments confirm the mathematical theory and elucidate various new features of filter performance as the Rossby number ε, the number of tracers L and the tracer noise variance change.

1

1 Introduction

Lagrangian tracers, such as floats and drifters, are usually the only source for many real-time data in the center of oceans [1, 2]. One key application of the Lagrangian data is the recovery of the current underlying velocity field. Motivated by this practical question, various approximate filters have been applied to Lagrangian data [3, 4, 5], and properties of these filters have been revealed through numerical experiments [6, 7].

Due to the nonlinear dynamics of the Lagrangian tracers, the classical analysis of the filters are carried out by numerical experiments, which in turn impedes systematic understanding. Fortunately, a recent work of the authors for random incompressible flows [8] established a clean theoretical framework for filtering noisy Lagrangian tracers by identifying the signal-observation system as a conditional Gaussian process despite the strong nonlinearity of the noisy tracer observations. Based on the theory of [9], the optimal filter is given by a Gaussian distribution with clean analytical formulas for the posterior mean and covariance involving Ricatti equations with random coefficients. In particular, when the underlying flow is incompressible, we show in [8] that the optimal filters have universal behavior when the tracer number L is large.

In geoscience, it is well known from real data that in mid-latitude, the slow varying geophysical flows are well approximated by geostrophically balanced (GB) flows [10, 11, 12, 13], which are incompressible. Thus it is tempting to apply the optimal filter constructed in [8] to the GB flows. Yet, this is an oversimplification. According to the mathematical explanation of the geostrophic approximation theory [14, 15], the compressible components in geophysical flows, gravity waves, do not really vanish, but rather decouple from the GB part and possess fast oscillating patterns in the limit of fast rotation, measured by ε, the Rossby number, satisfying $\varepsilon \ll 1$. It is due to the fast-wave averaging phenomenon that their contribution to the climate scale data vanishes. Whether the gravity waves can be ignored for filters remains elusive, because the Lagrangian tracers' dislocation, as the observation, depends nonlinearly upon the whole history of the gravity waves.

Motivated by the previous question, the first objective of the present paper is to understand the filtering skill of noisy Lagrangian tracers in a compressible random flow, and how much does it deviate from the incompressible scenario, which is well understood in [8]. The direct approach for this purpose is comparing filters derived for the two scenarios: a full filter that models the underlying flow as superposition of gravity waves and GB flow, and a GB filter that models the underlying flow as the former's projection to the GB parts. As verified below, both filters lie in the conditional Gaussian framework, hence possess concrete formulas. The gravity waves' impact over the filter can then be picked out and carefully analyzed through both mathematical theory and idealized numerical experiments which only involve quadrature of exact formulas.

The second motivation of present paper comes from a practical consideration. Filtering real turbulent flows in nature is rarely the same as numerical simulations. Most often, it is common practice to implement simplified imperfect filters involving only resolved scale dynamics, because the unresolved dynamics are too delicate to model and not of major concern. In the current context, a filter that recovers and requires only the GB flow dynamics is desired, as the gravity waves are too fast or noisy to be resolved. The simplest filter for this purpose is given by formal application of the GB filter's formulas to the tracers transported by the full flow. As the observations are also advected by gravity waves, the working conditions of the GB filter are actually violated. The potential error

in this imperfect filter must be analyzed with caution, since according to [16, 17, 18, 19], certain information may be impossible to recover due to modeling errors. On the other hand, the estimation of such errors characterizes the impact of the geostrophic approximation over Lagrangian data assimilation from a different perspective.

In this paper, a simplified setup is considered where a random rotating flow is modeled by a finite number of Fourier modes with random amplitudes:

$$\vec{v}(\vec{x}, t) = \sum_{\mathbf{k} \in \mathbf{K}} \hat{v}_{\mathbf{k}}(t) \exp(i\vec{k} \cdot \vec{x}) \vec{r}_{\mathbf{k}}, \tag{1.1}$$

where $\vec{k}$ is the wavenumber for index $\mathbf{k}$. The finite index set $\mathbf{K}$ splits into the GB subset $\mathbf{K}_B$ and the gravity subset $\mathbf{K}_g$, and each subset contains modes forming conjugate pairs so $\vec{v}$ is real-valued. Each $\hat{v}_{\mathbf{k}}(t)$ is modeled by an Ornstein-Uhlenbeck (O.U.) process:

$$d\hat{v}_{\mathbf{k}}(s) = (-d_{\mathbf{k}} + i\omega_{\mathbf{k}})\hat{v}_{\mathbf{k}}ds + f_{\mathbf{k}}ds + \sigma_{\mathbf{k}}dW_{\mathbf{k}}^v(s), \tag{1.2}$$

where $f_{\mathbf{k}}(s)$ is the deterministic forcing; $\omega_{\mathbf{k}}$ is zero for GB modes, i.e. $\mathbf{k} \in \mathbf{K}_B$, and of order reciprocal to the Rossby number ε for gravity modes, i.e. $\mathbf{k} \in \mathbf{K}_g$. On the other hand, the observation process is given by the trajectories of L Lagrangian tracers involving some noise, which are modeled by the following

$$\begin{aligned}
d\vec{X}_l(s) &= \vec{v}(\vec{X}_l(s), s)ds + \sigma_x dW_l^x(s) \\
&= \sum_{\mathbf{k} \in \mathbf{K}} \hat{v}_{\mathbf{k}}(t) \exp(i\vec{k} \cdot \vec{X}_l(s)) \vec{r}_{\mathbf{k}}ds + \sigma_x dW_l^x(s), \quad l = 1, \ldots, L. \tag{1.3}
\end{aligned}$$

Here $\sigma_x dW_l^x(s)$ models the combined effects of random perturbation from the turbulent flow and the intrinsic instrumental noise, since $\vec{v}$ is essentially a Galerkin truncation of a real turbulence which has a residual part that is not accounted. In the standard terminology of filtering, $\sigma_x dW_l^x(s)$ can be seen as an observation noise.

The fundamental mathematical observation [8] which forms the basis for further analysis here is that the full signal-observation system $(\vec{v}_{\mathbf{k}}(s), \mathbf{k} \in \mathbf{K}; \vec{X}_l(s), l \leq L)$ is a conditional Gaussian process, as they are jointly linearly once the observations $\vec{X}_l(s)$ are fixed. Therefore by [9] the optimal filter is given by a Gaussian distribution $\pi_{s|s} = \mathcal{N}(m_s, R_s)$, where m_s, R_s follow explicit differential equations. As $\pi_{s|s}$ includes both GB part and gravity waves in its model, it will be named as the full or perfect filter. It can tell us the uncertainty reduced by Lagrangian tracers, for both the geostrophic and gravity wave parts of the flow, and can be used to quantify the error made by the simplified filter.

By applying the geostrophic approximation, (1.1) and (1.3) are projected to their GB part:

$$\vec{v}^B(\vec{x}, t) = \sum_{\mathbf{k} \in \mathbf{K}_B} \hat{v}_{\mathbf{k}}(t) \exp(i\vec{k} \cdot \vec{x}) \vec{r}_{\mathbf{k}}, \quad d\vec{X}_l^B(s) = \vec{v}^B(\vec{X}_l^B(s), s)ds + \sigma_x dW_l^x(s). \tag{1.4}$$

Like the full model, $(\vec{v}_{\mathbf{k}}(s), \mathbf{k} \in \mathbf{K}_B; \vec{X}_l^B(s), l \leq L)$ jointly form a conditional Gaussian process, hence the optimal filter is given by a Gaussian distribution $\pi_{s|s}^G = \mathcal{N}(m_s^G, R_s^G)$, which will be named as the GB filter. Since $\vec{v}_s^B$ is incompressible, the results of [8] can be directly applied to the GB filter, i.e. 1) $\vec{X}_l^B(s)$ has uniform distribution on $\mathbb{T}^2 = [-\pi, \pi]^2$ as their invariant distribution; 2) the uncertainty reduction grows on the order of $\ln L$ for increasing L. If the full filter behaves similarly to the GB filter, then the previous results

provide a good reference for understanding filters of compressible flows and the role of gravity waves as the Rossby number varies.

The imperfect filter that utilizes only the GB modes' dynamics is obtained by applying the formulas of the GB filter to the observations from the full model, i.e. the observations $\vec{X}_1(s), \ldots, \vec{X}_L(s)$ are used as input for the GB filter. Evidently the assumptions of conditional Gaussian theory are not valid, so the output produced, denoted by $\pi^r_{s|s}$, is a reduced sub-optimal filter. This mimics the scenario that frequently happens in reality, that is an over simplified model is applied to a complicated object. Yet it is sometimes the only available choice for filtering because: 1) it uses only the resolved dynamics of GB flow which is sometimes the only available dynamics; 2) it is computationally much more efficient than the full filter. The precision of this reduced filter can be measured by its difference with the GB part of the full filter $\pi_{s|s}$.

As the full, GB and reduced filters all follow concrete formulas, their differences can be studied by both simple numerics and rigorous math. Recall that in [11, 14, 20] the rigorous validation of the geostrophic adjustment theory requires that $\varepsilon \ll 1$, i.e. a fast rotational scenario. Hence intuitively, the key parameter here is the Rossby number ε, and the geostrophic approximation should make little difference in the filters when ε is small. By exploiting the fast-wave averaging phenomenon of gravity waves, this claim is validated in a mathematical proof below showing the differences between the filters are scaled with ε for any finite moments. In other words, when the ambient rotation is fast

- The geostrophic approximation makes little difference for the recovery of GB flow using Lagrangian tracers;

- The behavior of GB filter, which is well understood in [8], is a good reference for Lagrangian data assimilation in a rapidly rotating compressible flow.

Corresponding numerical experiments implemented with different combinations of Rossby number ε, the number of tracers L, and observation noise strength σ_x not only validate our claims, but also reveal the joint effect of the observation parameters and fundamental differences between filtering in slow and fast rotational regimes.

The remainder of this paper is arranged as follows: in Section 2, we formulate a random rotating shallow water equation explicitly as an example for the general filtering framework while the full filter, the GB filter and the reduced filter are carefully derived. In Section 3 we offer a rigorous mathematical explanation of our key finding while the detailed proofs are left to Section 4. Section 5 reports on the numerical experiments and comparison of the filters with different Rossby number ε. For readers interested in new phenomena rather than the detailed proof, Section 4 can be skipped in a first reading. Section 6 concludes this paper while discussing issues related to this topic.

2 Basic set-up

2.1 Random rotating compressible shallow water flows

To begin with, a random two dimensional rotating compressible shallow water velocity field $\vec{v}$ with corresponding height function $h \in \mathbb{R}$ is formulated below as an explicit example of the general setup (1.1):

$$\begin{bmatrix} \vec{v}(\vec{x},t) \\ h(\vec{x},t) \end{bmatrix} = \sum_{\vec{k} \in \mathbf{K}, \alpha \in \{0,\pm\}} \hat{v}_{\vec{k},\alpha}(t) \exp(\mathrm{i}\vec{k} \cdot \vec{x}) \vec{r}_{\vec{k},\alpha}. \tag{2.1}$$

Here $\mathbf{K}$ is some finite symmetric subset of $\mathbb{Z}^2$, while modes with $\alpha = 0$ represent the geostrophically balanced (GB) part and modes with $\alpha = \pm$ represent the gravity waves. The vectors $\vec{r}_{\vec{k},\alpha}$ are the eigenvectors associated with different modes, where the projection of $\vec{r}_{\vec{k},0}$ on the velocity components is perpendicular to $\vec{k}$ [12, 14, 15] due to the incompressibility of the GB part and $\vec{r}_{\vec{k},\pm}$ indicate the direction of the compressible gravity wave. To model the stochastic nature of all these modes, we drive the random amplitudes $\hat{v}_{\vec{k},\alpha}(s)$ with stochastic forcing and damping terms that stabilize the system:

$$
\begin{aligned}
\mathrm{d}\hat{v}_{\vec{k},0}(t) &= \left(-d_B \hat{v}_{\vec{k},0} + f_{\vec{k},0}(t) \right)\mathrm{d}t + \sigma_{\vec{k},0}\mathrm{d}W_{\vec{k},0}(t), \\
\mathrm{d}\hat{v}_{\vec{k},\pm}(t) &= \left((-d_g + \mathrm{i}\omega_{\vec{k},\alpha})\hat{v}_{\vec{k},\pm}(t) + f_{\vec{k},\pm}(t) \right)\mathrm{d}t + \sigma_{\vec{k},\pm}\mathrm{d}W_{\vec{k},\pm}(t).
\end{aligned}
\tag{2.2}
$$

Here d_B, d_g are both positive numbers and notice that (2.2) also contains deterministic forcing. In order for (2.1) to be real-valued, we require that $\vec{r}_{\vec{k},\alpha}^* = \vec{r}_{-\vec{k},-\alpha}$ and $(\hat{v}_{\vec{k},\alpha})^* = \hat{v}_{-\vec{k},-\alpha}$. The first conjugation equality is met by the detailed formulation of $\vec{r}_{\vec{k},\alpha}$ below and the second conjugation equality can be enforced by requiring each term in (2.2) to form conjugate pairs. For a detailed description of this enforcement, we refer to Appendix A.1 of [8]. Such a modeling strategy for turbulence has also been applied in general in [21].

In order to understand the intuition behind this model and to see the natural choice of $\vec{r}_{\vec{k},\alpha}$ and $\omega_{\vec{k},\alpha}$, recall the non-dimensional linearized shallow water equation, Section 4.4 [12]:

$$
\begin{aligned}
\frac{\partial \vec{u}}{\partial t} + \varepsilon^{-1}\vec{u}^\perp &= -\varepsilon^{-1}\nabla\eta, \\
\frac{\partial \eta}{\partial t} + \varepsilon^{-1}\delta\nabla \cdot \vec{u} &= 0.
\end{aligned}
\tag{2.3}
$$

Here $\vec{u}$ is a horizontal two dimensional velocity field and η is the height function. We denote the non-dimensional parameters $\varepsilon = \mathrm{Ro}, \delta = \mathrm{Ro}^2\mathrm{Fr}^{-2}$ with Ro being the Rossby number which represents the ratio between the Coriolis term and the advection term, and Fr being the Froude number. For most atmosphere-ocean problems, ε is a small number representing fast rotation and δ is either $O(1)$ or $O(\varepsilon)$. Following Section 4.4 of [12], the general solution of (2.3) is given by a superposition of plane waves:

$$
\begin{bmatrix} \vec{u}(\vec{x},t) \\ \eta(\vec{x},t) \end{bmatrix} = \sum_{\vec{k}\in\mathbb{Z}^2,\alpha\in\{0,\pm\}} \hat{u}_{\vec{k},\alpha} \exp(\mathrm{i}\vec{k}\cdot\vec{x} - \mathrm{i}\omega_{\vec{k},\alpha}t)\vec{r}_{\vec{k},\alpha}.
\tag{2.4}
$$

The modes with $\alpha = 0$ represent the geostrophically balanced (GB) modes, also known as the vortical waves. The geostrophic balance relation $\vec{u}^\perp = -\nabla\eta$ always holds [12]. The associated rotational speed $\omega_{\vec{k},0} = 0$ and the normalized eigenvector $\vec{r}_{\vec{k},0}$ is given by

$$
\vec{r}_{\vec{k},0} = \frac{1}{\sqrt{|\vec{k}|^2 + 1}} \begin{bmatrix} -\mathrm{i}k_2 \\ \mathrm{i}k_1 \\ 1 \end{bmatrix}.
\tag{2.5}
$$

The modes with $\alpha = \pm$ represent the gravity modes also known as the Poincaré waves [12]. They have a nonzero phase speed:

$$
\omega_{\vec{k},\pm} = \pm\varepsilon^{-1}\sqrt{\delta|\vec{k}|^2 + 1}.
\tag{2.6}
$$

The associated normalized eigenvectors $\vec{r}_{\vec{k},\pm}$ are given by

$$\vec{r}_{\vec{k},\pm} = \frac{1}{|\vec{k}|\sqrt{(\delta + \delta^2)|\vec{k}|^2 + 2}} \begin{bmatrix} ik_2 \pm k_1\sqrt{\delta|\vec{k}|^2 + 1} \\ -ik_1 \pm k_2\sqrt{\delta|\vec{k}|^2 + 1} \\ \delta|\vec{k}|^2 \end{bmatrix}. \tag{2.7}$$

For the special case, $\vec{k} = \vec{0}$, the Poincaré waves have no gravity component and coincide with the inertial waves. The resulting eigenvalues become $\omega_{\vec{0},\pm} = \pm\varepsilon^{-1}$ with the eigenvectors

$$\vec{r}_{\vec{0},+} = \frac{1}{\sqrt{2}} \begin{bmatrix} i \\ 1 \\ 0 \end{bmatrix} \quad \text{and} \quad \vec{r}_{\vec{0},-} = \frac{1}{\sqrt{2}} \begin{bmatrix} -i \\ 1 \\ 0 \end{bmatrix}.$$

By taking a finite Fourier truncation and replacing the deterministic coefficients $\hat{u}_{\vec{k},\alpha} \exp(-i\omega_{\vec{k},\alpha}t)$, in (2.4) with the stochastic processes $\vec{v}_{\vec{k},\alpha}$ modeled by (2.2), we arrive at the basic rotating compressible random field model in (2.1)-(2.2). The additional linear coefficient $i\omega_{\vec{k},\alpha}$ from (2.6) for the gravity waves model their oscillations, which are fast for $\varepsilon \ll 1$. It is worth noticing that the Rossby number ε and δ enter the dynamics only through the gravity waves: they appear only in $\vec{r}_{\vec{k},\pm}$ and $\omega_{\vec{k},\pm}$. Moreover, $\omega_{\vec{k},\pm}$ is a parameter of order ε^{-1}; its appearance in the linear coefficient for the gravity modes, (2.2), represents the same rotational effect as in the deterministic setting.

2.2 Filters for noisy Lagrangian tracers

We consider the random rotating compressible flows defined in (1.1) and (1.2). Evidently, the stochastic processes $\{\hat{v}_{\mathbf{k}}\}$ is the signal process we need to recover. For better illustration, group all the signals from balanced geostrophic modes into a column vector process $\mathbf{U}_s^B$ and likewise the gravity modes into $\mathbf{U}_s^g$. They jointly form a full signal column vector process $\mathbf{U}_s$. Regarding notation, we will assign the superscript B for the GB parts, and g for the gravity parts. The dynamics of these signal process, according to (2.1) and (2.2), can be regrouped and written as:

$$d\mathbf{U}_s^B = -\Gamma^B \mathbf{U}_s^B ds + F_s^B ds + \Sigma_u^B dW_u^B(s), \tag{2.8}$$

$$d\mathbf{U}_s^g = (-\Gamma^g + i\Omega_\varepsilon)\mathbf{U}_s^g ds + F_s^g ds + \Sigma_u^g dW_u^g(s), \tag{2.9}$$

and jointly:

$$d\mathbf{U}_s = -\Gamma\mathbf{U}_s ds + F_s ds + \Sigma_u dW_u(s). \tag{2.10}$$

Here Ω_ε is diagonal with $\mathbf{k}$-$\mathbf{k}$th entry

$$\omega_{\mathbf{k}} = \pm\varepsilon^{-1}\sqrt{\delta|\vec{k}|^2 + 1}, \qquad \mathbf{k} \in \mathbf{K}_g. \tag{2.11}$$

The velocity field generated by the two parts can be written down as:

$$\vec{v}^B(\vec{x}, s) = P_X^B(\vec{x})\mathbf{U}_s^B, \quad \vec{v}^g(\vec{x}, s) = P_X^g(\vec{x})\mathbf{U}_s^g.$$

with

$$P_X^H(\vec{x}) = [\cdots, \exp(i\vec{k} \cdot \vec{x})\vec{r}_{\mathbf{k}}, \cdots]_{\mathbf{k} \in \mathbf{K}_H}, \quad H = B, g.$$

Their sum is the full flow:

$$\vec{v}(\vec{x}, s) = \vec{v}^B(\vec{x}, s) + \vec{v}^g(\vec{x}, s) = P_X(\vec{x})\mathbf{U}_s, \quad P_X = [P_X^B, P_X^g].$$

Therefore, it is equivalent to know the flow field $\vec{v}, \vec{v}^B$ or the signal process $\mathbf{U}, \mathbf{U}^B$ respectively.

Assuming that the deterministic forcing F_s is periodic, the signal process $\mathbf{U}_t$ has an equilibrium distribution, which is Gaussian $\pi_t^{att} = \mathcal{N}(m_t^{att}, R_{att})$. Using the Fokker-Plank equation, the equilibrium mean and covariance are given by:

$$m_t^{att} = \int_{-\infty}^t \exp(-\Gamma(t-s))F_s\mathrm{d}s, \quad R_{att} = [2\mathrm{Re}(\Gamma)]^{-1}\Sigma_u\Sigma_u^*.$$

As the GB marginal of $\mathbf{U}_t$, $\mathbf{U}_t^B$ has an equilibrium distribution $\pi_{B,t}^{att}$ being the marginal distribution of π_t^{att} for the GB part. Notably, without any observation, π_t^{att} and $\pi_{B,t}^{att}$ give the least biased states of $\mathbf{U}_t$ and $\mathbf{U}_t^B$ respectively. They naturally serve as the initial state of the filters. And due to the chaotic nature of random flows in nature, they contain generally little information.

Given one realization of the velocity field $\vec{v}_{t\geq 0}$, the trajectory of each one of the L noisy Lagrangian tracers advected by the full flow follows the stochastic differential equation (SDE):

$$\mathrm{d}\vec{X}_l(s) = P_X(\vec{X}_l(s))\mathbf{U}_s\mathrm{d}s + \sigma_x\mathrm{d}W_l^x(s).$$

Group all $\vec{X}_l(s)$ together as

$$\mathbf{X}_s = \begin{bmatrix} \vec{X}_1(s) \\ \vdots \\ \vec{X}_L(s) \end{bmatrix}.$$

This observation process follows:

$$\mathrm{d}\mathbf{X}_s = \mathbf{P}_X(\mathbf{X}_s)\mathbf{U}_s\mathrm{d}s + \sigma_x\mathrm{d}W_s^x, \tag{2.12}$$

with

$$\mathbf{P}_X(\mathbf{X}_s) = \begin{bmatrix} P_X(\vec{X}_1(s)) \\ \vdots \\ P_X(\vec{X}_L(s)) \end{bmatrix} = \begin{bmatrix} \cdots & \exp(i\vec{k}\cdot\vec{X}_1(s))\vec{r}_\mathbf{k} & \cdots \\ \vdots & \vdots & \vdots \\ \cdots & \exp(i\vec{k}\cdot\vec{X}_L(s))\vec{r}_\mathbf{k} & \cdots \end{bmatrix} = [\mathbf{P}_X^B(\mathbf{X}_s), \mathbf{P}_X^g(\mathbf{X}_s)].$$

On the other hand, by formally applying mode reduction over the gravity waves, one models the random flow using $\vec{v}^B$ only. Hence a noisy Lagrangian tracer drifted by the GB flow $\vec{v}^B$ follows SDE:

$$\mathrm{d}\vec{X}_l^B(s) = P_X^B(\vec{X}_l^B(s))\mathbf{U}_s^B\mathrm{d}s + \sigma_x\mathrm{d}W_l^x(s).$$

For L tracers, group them together as $\mathbf{X}_s^B$, then

$$\mathrm{d}\mathbf{X}_s^B = \mathbf{P}_X^B(\mathbf{X}^B(s))\mathbf{U}_s^B\mathrm{d}s + \sigma_x\mathrm{d}W_s^x. \tag{2.13}$$

2.2.1 Full optimal filter

$\mathbf{U}_s, \mathbf{X}_s$ jointly form the signal-observation process of the full model. Their joint evolution, (2.10) and (2.12), is linear once the observation process $\mathbf{X}_{t \le T}$ is given. If moreover, the initial prior distribution for $\mathbf{U}_0$ is given by a Gaussian distribution, say π_0^{att}, then $(\mathbf{U}_s, \mathbf{X}_s)$ is qualified to be a conditional Gaussian process as described in detail in [8] for the incompressible case. By Theorem 12.7 of [9], the conditional distribution of $\mathbf{U}_t$ given the value of $\mathbf{X}_{t \le T}$ is given by the Gaussian distribution $\pi_{t|t} = \mathcal{N}(m_t, R_t)$, where m_t, R_t solve the following equation:

$$\mathrm{d}m_t = [-\Gamma m_t + F_t]\mathrm{d}t + \sigma_x^{-1} R_t \mathbf{P}_X^*(\mathbf{X}_t)[\mathrm{d}\mathbf{X}_t - \mathbf{P}_X(\mathbf{X}_t)m_t\mathrm{d}t], \qquad (2.14)$$

$$\mathrm{d}R_t = [-\Gamma R_t - R_t\Gamma + \Sigma_u\Sigma_u^* - \sigma_x^{-2} R_t \mathbf{P}_X^*(\mathbf{X}_t)\mathbf{P}_X(\mathbf{X}_t)R_t]\mathrm{d}t. \qquad (2.15)$$

As we will be interested in the GB part of this filter, we will decompose vectors and matrices into sub-vectors and sub-matrices with indices in either $\mathbf{K}_B$ or $\mathbf{K}_g$:

$$\mathbf{U}_t = \begin{bmatrix} \mathbf{U}_t^B \\ \mathbf{U}_t^g \end{bmatrix}, \quad m_t = \begin{bmatrix} m_t^B \\ m_t^g \end{bmatrix}, \quad R_t = \begin{bmatrix} R_t^B, & S_t \\ S_t^*, & R_t^g \end{bmatrix}. \qquad (2.16)$$

Therefore, the conditional law for $\mathbf{U}_t^B$ given $\mathbf{X}_{t \le T}$ is $\mathcal{N}(m_t^B, R_t^B)$.

2.2.2 Geostrophically balanced (GB) filter

By applying the geostrophic approximation, one can model the velocity field using $\vec{v}^B$ and noisy Lagrangian tracers using $\vec{X}_l^B(s)$. The GB signal-observation system $(\mathbf{U}_s^B, \mathbf{X}_s^B)$ is conditional Gaussian again because (2.8) and (2.13) are jointly linear conditioned on $\mathbf{X}_s^B$ as developed in detail in [8]. The conditional distribution of $\mathbf{U}_t^B$ given observation of $\mathbf{X}_{t \ge 0}^B$ is $\mathcal{N}(m_t^G, R_t^G)$, where (m_t^G, R_t^G) are solutions to the following:

$$\mathrm{d}m_t^G = [-\Gamma^B m_t^G + F_t^B]\mathrm{d}t + \sigma_x^{-1} R_t^G \mathbf{P}_X^{B*}(\mathbf{X}_s^B)[\mathrm{d}\mathbf{X}_s^B - \mathbf{P}_X^B(\mathbf{X}_s^B)m_t^G\mathrm{d}t], \qquad (2.17)$$

$$\mathrm{d}R_t^G = [-\Gamma^B R_t^G - R_t^G\Gamma^B + \Sigma_u^B\Sigma_u^{B*} - \sigma_x^{-2} R_t^B \mathbf{P}_X^{B*}(\mathbf{X}_s^B)\mathbf{P}_X^B(\mathbf{X}_s^B)R_t^B]\mathrm{d}t. \qquad (2.18)$$

We will assign the superscript G to every process related to this GB filter. By definition, we can write $\pi_{t|t}^G = \Pi_t^G(\mathbf{X}_{t \le T}^B)$, i.e. the optimal filter is a function of the observation process $\mathbf{X}_{t \le T}^B$.

As mentioned in Section 1, because $\vec{v}_s^B$ is incompressible, all the results of [8] are applicable to this GB filter. The clear knowledge of the GB filter's behavior listed in Section 1 will be frequently referred to in order to understand the fundamental difference made by the compressibility of the flows and how they depend on the Rossby number ε.

Note that this filter is an optimal perfect filter for the geostrophically balanced flow. However the GB filter requires the Lagrangian trajectories of the GB flow field alone as the observations. Such observations of trajectories due to the GB part of the flow are inaccessible practically; actually only noisy Lagrangian trajectories associated with the full rotating compressible flow field are observed in practice. This motives the reduced filter discussed next.

2.2.3 Reduced Filter

A reduced filter can be obtained by inputting the GB filter with noisy tracer observations from the full compressible model, i.e. let $\pi_{t|t}^r = \Pi_t^G(\mathbf{X}_{t \leq T})$. According to the setup of the GB filter, $\pi_{t|t}^r = \mathcal{N}(m_t^r, R_t^r)$ with (m_t^r, R_t^r) following (2.17) and (2.18) while the observation $\mathbf{X}_t^B$ there is replaced by $\mathbf{X}_t$. In other words, they follow:

$$\mathrm{d}m_t^r = -\Gamma^B m_t^r \mathrm{d}t + F_t^B \mathrm{d}t + \sigma_x^{-2} R_t^r \mathbf{P}_X^{B*}(\mathbf{X}_t)[\mathrm{d}\mathbf{X}_t - \mathbf{P}_X^B(\mathbf{X}_t)m_t^r \mathrm{d}t], \qquad (2.19)$$

$$\mathrm{d}R_t^r = [-\Gamma^B R_t^r - R_t^r \Gamma^B + \Sigma_u^B \Sigma_u^{B*} - \sigma_x^{-2} R_t^r \mathbf{P}_X^{B*}(\mathbf{X}_s)\mathbf{P}_X^B(\mathbf{X}_s)R_t^r]\mathrm{d}t. \qquad (2.20)$$

Unlike the previous two filters, $\pi_{t|t}^r$ is not the optimal filter for $\mathbf{U}_t^B$ given $\mathbf{X}_{t \leq T}$, since when we know the GB part of $\pi_{t|t}$, $\mathcal{N}(m_t^B, R_t^B)$, is the optimal filter in this case. $\pi_{t|t}^r$ can be interpreted as an imperfect filter obtained by geostrophic approximation. Nevertheless, it is possible that $\pi_{t|t}^r$ is a close approximation to the optimal filter. In that case, the reduced dynamics is safe to apply for a Lagrangian tracers' filter.

2.2.4 Uncertainty Reduction

One practical question in filtering is how much uncertainty is reduced by one filter compared with the unfiltered velocity field, meaning the absence of observations. Here the prior distribution is given by the equilibrium distribution π_t^{att}, with mean $\vec{m}_t^{att}$ and covariance R_{att}. Empirical information theory, as in [17, 18, 22, 23], is applied to measure this uncertainty reduction.

In the information-theoretic framework, one natural way to measure the lack of information in one probability density q, when the real distribution is p, is through the relative entropy

$$\mathcal{P}(p, q) = \int p \ln \frac{p}{q}.$$

For our purposes, of key importance is the so-called Bayesian-update interpretation of relative entropy. It states that if $p = \pi_{t|t}$ is a posterior distribution conditioned on the observation $\mathbf{X}_{t \leq T}$ and q is the corresponding prior distribution, which is the case for $q = \pi_t^{att}$, then $\mathcal{P}(\pi_{t|t}, \pi_t^{att})$ measures the additional information beyond π_t^{att} gained by having observed $\mathbf{X}_{t \leq T}$, namely, the uncertainty reduction. Likewise, $\mathcal{P}(\pi_{t|t}^G, \pi_{B,t}^{att})$ measures the additional information from $\mathbf{X}_{t \leq T}^B$ for $\mathbf{U}_s^B$.

In the present paper, a special formula of relative entropy for Gaussian distributions is particularly useful. Consider $p \sim \mathcal{N}(\vec{m}_p, R_p)$ and $q \sim \mathcal{N}(\vec{m}_q, R_q)$ are Gaussian, the relative entropy is [24, 25]:

$$\mathcal{P}(p, q) = \left[\tfrac{1}{2}(\vec{m}_p - \vec{m}_q)^T R_q^{-1}(\vec{m}_p - \vec{m}_q)\right] + \tfrac{1}{2}\left[\mathrm{tr}(R_p R_q^{-1}) - N - \ln\det(R_p R_q^{-1})\right], \quad (2.21)$$

where N is the dimension of both the distributions. The first term in brackets in (2.21) is called the "signal", it measures the lack of information in the mean weighted by model covariance; the second term in brackets is called the "dispersion" and involves only the covariance ratio. For our filtering application, (2.21) can be directly applied to compute $\mathcal{P}(\pi_{t|t}, \pi_t^{att})$ and $\mathcal{P}(\pi_{t|t}^G, \pi_{B,t}^{att})$. This is because the complex-valued processes form conjugate pairs, interested readers are directed to Appendix A.2 of [8] for detailed validations.

3 Difference between filters in the small Rossby number limit

Following the discussion of Section 1, the impact of the geostrophic approximation over filtering can be measured by the differences between the GB part of full filter (m_t^B, R_t^B) (2.14)-(2.15), the GB filter (m_t^G, R_t^G) (2.17)-(2.18), and the reduced filter (m_t^r, R_t^r) (2.19)-(2.20). The objective of this section is to state theorems showing that these differences are small when the Rossby number $\varepsilon \ll 1$.

As we will be interested in the limiting behavior as $\varepsilon \to 0$, it is necessary for us to think of families of processes parameterized by ε. Notice that the Rossby number ε and the ratio δ do not enter the equation of GB flow $\mathbf{U}_s^B$ as in (2.8); it is intuitive to fix a realization of $\mathbf{U}_{t\geq0}^B$, or equivalently $\vec{v}_{t\geq0}^B$ while changing the value of ε, δ. As a result, for each fixed realization of $\vec{v}_{t\geq0}^B$, a family of $\mathbf{U}_{t\geq0}^g$ is coupled with it. For this purpose, in certain situations the conditional distribution with a given realization of $\vec{v}_{t\geq0}^B$ is considered, which is denoted as $\mathbb{P}_{\vec{v}^B}$. For a.e. realization of $\vec{v}_{t\geq0}^B$, $\mathbf{U}_{t\leq T}^B$ is a bounded deterministic process under $\mathbb{P}_{\vec{v}^B}$. On the other hand, when one averages over all realization of $\vec{v}_{t\geq0}^B$, the corresponding probability will be called the super-ensemble probability $\mathbb{P}$.

Remark 3.1. *Technically speaking, the conditional distribution $\mathbb{P}_{\vec{v}^B}$ defined here is a regular conditional distribution, and its existence is due to the fact that the spaces we considered here, $\mathbb{R}$ and $C[0,t]$, are Polish under the uniform metric. For the technical details, we refer to Theorems 6.3 and A1.1 of [26].*

3.1 Statements of theorems

In order for two filters to have comparable results, it is necessary to require that they have comparable initial conditions. An assumption over initial condition is defined:

Assumption 3.2. *For a filter $\pi_{t|t} = \mathcal{N}(m_t, R_t)$ of the full modes and a filter $\tilde{\pi}_{t|t} = \mathcal{N}(\tilde{m}_t, \tilde{R}_t)$ of the GB modes, we say their initial values are comparable if*

$$m_0^B = \tilde{m}_0, \quad R_0^B = \tilde{R}_0, \quad S_0 = 0.$$

Here we use the decomposition as stated in (2.16), so it is assumed that there is no correlation in the initial data between the GB modes and the gravity modes.

It is easy to check that the full filter, GB filter and reduced filter meet this requirement if the equilibrium measures, π_0^{att} and $\pi_{B,0}^{att}$, are used as initial condition. Our first result studies the difference between the optimal filter for $\mathbf{U}_t$ given $\mathbf{X}_{t\leq T}$ and the reduced filter:

Theorem 3.3. *Suppose both the full filter (2.14)-(2.15) and the reduced filter (2.19)-(2.20) are started with comparable initial conditions as Assumption 3.2 states, then for any fixed $q \geq 1, T > 0$, the geostrophically balanced (GB) part of the full filter $(m_{t\leq T}^B, R_{t\leq T}^B)$ and the reduced filter $(m_{t\leq T}^r, R_{t\leq T}^r)$ have their difference bounded by the following moment constraints with a proper ε-uniform constant $M = M(q,T)$:*

(i) $[\mathbb{E}\sup_{t\leq T} \|R_t^B - R_t^r\|^{2q}]^{\frac{1}{2q}} \leq \varepsilon M$;

(ii) $[\mathbb{E}\sup_{t\leq T} |m_t^B - m_t^r|^q]^{\frac{1}{q}} \leq \varepsilon M$.

Moreover, both claims hold when $\mathbb{E}$ is replaced by the conditional distribution with given realization of $\vec{v}_{t \geq 0}^B$, i.e. $\mathbb{E}_{\vec{v}^B}$, for a.s. $\vec{v}_{t \geq 0}^B$. However the ε-uniform constant M may depend on $\vec{v}_{t \geq 0}^B$ in this case.

The second results regards a similar phenomenon for the difference between the GB filter and full filter:

Theorem 3.4. *Suppose the full filter (2.14)-(2.15) and the GB filter (2.17)-(2.18) are started with comparable initial conditions as Assumption 3.2 states. Suppose the probability space of the two filters are coupled so that the GB part of full flow, $\vec{v}_{t \geq 0}^B$, coincides with the flow of the GB filter and the stochastic forcing driving the tracers in two flows, W_s^x in (2.12) and (2.13) are identical, then for any $q \geq 1, T > 0$, the GB part of the full filter $(m_{t \leq T}^G, R_{t \leq T}^G)$ and the GB filter $(m_{t \leq T}^G, R_{t \leq T}^G)$ have their difference bounded by the following moment constraints with a proper ε-uniform constant $M = M(q, T, \vec{v}_{s \geq 0}^B)$:*

(i) $[\mathbb{E}_{\vec{v}^B} \sup_{t \leq T} \|R_t^B - R_t^G\|^{2q}]^{\frac{1}{2q}} \leq \varepsilon M$;

(ii) $[\mathbb{E}_{\vec{v}^B} \sup_{t \leq T} |m_t^B - m_t^G|^q]^{\frac{1}{q}} \leq \varepsilon M$.

Both claims hold for a.e. realization of $\vec{v}_{t \geq 0}^B$.

3.2 Mathematical framework: uniformly bounded moments

As the differences between stochastic processes are our major concern, fixing particular norms will be helpful. Two relative strong and standard norms for stochastic processes are the $L^q(\Omega, [0, T])$ norm and $L^q(\Omega, C([0, T]))$ norm with a $q \geq 1$, which are defined by:

$$\|x_{t \leq T}\|_{L^q([0,T])} = \left[\mathbb{E}_{\mathbb{Q}} \int_0^T |x_t|^q \mathrm{d}t \right]^{\frac{1}{q}}, \quad \|x_{t \leq T}\|_{L^q(\Omega, C([0,T]))} = \left[\mathbb{E}_{\mathbb{Q}} \sup_{t \leq T} |x_t|^q \right]^{\frac{1}{q}}.$$

Here x_t can be scalar, vector or matrix valued, and $|\cdot|$ is the corresponding norm for different spaces; the spectral norm is applied for matrices in this case.

For sake of brevity, T will be fixed as a constant in the following and we write L^q for $L^q(\Omega, [0, T])$, L_C^q for $L^q(\Omega, C([0, T]))$. As we will consider time intervals of finite length, L_C^q-norm is a stronger norm than L^q-norm.

We will say a family of stochastic processes $\{x_{t \leq T}^\varepsilon\}$ parameterized by $\varepsilon > 0$ under a probability measure $\mathbb{Q}$ is

1. ε-uniformly $\mathbb{Q}$-a.s. bounded, if there exists an M such that $|x_s^\varepsilon| \leq M$, $\mathbb{Q}$-a.s. for all $t \leq T, \varepsilon > 0$;

2. ε-uniformly bounded in L^q (or L_C^q) under $\mathbb{Q}$, if there exists an M so $\|x_{t \leq T}\|_{L^q} \leq M$ (or $\|x_{t \leq T}\|_{L_C^q} \leq M$);

3. of order ε^d in L^q or L_C^q under $\mathbb{Q}$, if $\{\varepsilon^{-d} x_{t \leq T}^\varepsilon\}$ is ε-uniformly bounded in L^q or L_C^q respectively.

For example, the first claim of Theorem 3.3 can be stated as $\|R_t^r - R_t^B\|$ is of order ε in L_C^{2q}; the other claims of two theorems can also be stated in similar fashion. Occasionally we also consider a family of random variables, rather than random processes, and then the definitions above can be easily generalized under the norm $\|X\|_{L^q} = (\mathbb{E} X^q)^{1/q}$.

The following lemma states the basic arithmetic properties of these concepts; we will use it without detailed referencing in the following as it is applied frequently.

Lemma 3.5. *Fix any $q \geq 1$, let $\{v_{t \leq T}^{\varepsilon}\}$ be ε-uniformly $\mathbb{Q}$-a.s. bounded; $\{w_{t \leq T}^{\varepsilon}\}, \{x_{t \leq T}^{\varepsilon}\}$ be ε-uniformly bounded in L_C^q under $\mathbb{Q}$; $\{y_{t \leq T}^{\varepsilon}\}, \{z_{t \leq T}^{\varepsilon}\}$ be ε-uniformly bounded in L^q under $\mathbb{Q}$. Then the following hold under $\mathbb{Q}$:*

1. *$\{v_{t \leq T}^{\varepsilon}\}$ is ε-uniformly bounded in L_C^q; $\{w_{t \leq T}^{\varepsilon}\}$ is ε-uniformly bounded in L^q;*

2. *$\{x_s^{\varepsilon} + w_s^{\varepsilon}\}$ is ε-uniformly bounded in L_C^q; $\{y_s^{\varepsilon} + z_s^{\varepsilon}\}$ is ε-uniformly bounded in L_C^q;*

3. *$\{v_s^{\varepsilon} x_s^{\varepsilon}\}$ is ε-uniformly bounded in L_C^q; $\{v_s^{\varepsilon} y_s^{\varepsilon}\}$ is ε-uniformly bounded in L^q;*

4. *$\{w_s^{\varepsilon} x_s^{\varepsilon}\}$ is ε-uniformly bounded in $L_C^{\frac{q}{2}}$; $\{y_s^{\varepsilon} z_s^{\varepsilon}\}$ is ε-uniformly bounded in $L^{\frac{q}{2}}$;*

5. *If $q \geq 2$, $\{\int_0^s y_r^{\varepsilon} z_r^{\varepsilon} \mathrm{d}r\}$ is ε-uniformly bounded in $L_C^{\frac{q}{2}}$.*

Proof. The first three claims are just verification of the definitions using Minkowski inequality. For the fourth, apply Cauchy Schwarz:

$$\mathbb{E}_{\mathbb{Q}} \sup_{t \leq T} |w_s^{\varepsilon} x_s^{\varepsilon}|^{\frac{q}{2}} \leq \mathbb{E}_{\mathbb{Q}} \sup_{t \leq T} |w_s^{\varepsilon}|^{\frac{q}{2}} \sup_{t \leq T} |x_s^{\varepsilon}|^{\frac{q}{2}} \leq \left[\mathbb{E}_{\mathbb{Q}} \sup_{t \leq T} |w_s^{\varepsilon}|^q \mathbb{E}_{\mathbb{Q}} \sup_{t \leq T} |x_s^{\varepsilon}|^q \right]^{\frac{1}{2}};$$

$$\mathbb{E}_{\mathbb{Q}} \int_0^T |y_s^{\varepsilon} z_s^{\varepsilon}|^{\frac{q}{2}} \mathrm{d}s \leq \mathbb{E}_{\mathbb{Q}} \int_0^T |y_s^{\varepsilon}|^q \mathrm{d}s \, \mathbb{E}_{\mathbb{Q}} \int_0^t |z_s^{\varepsilon}|^q \mathrm{d}s.$$

The fifth claim comes by applying Young's inequality, Minkowski inequality and Hölder's inequality in a sequel:

$$\left[\sup_{t \leq T} \int_0^t y_s^{\varepsilon} z_s^{\varepsilon} \mathrm{d}s \right]^{\frac{q}{2}} \leq \left[\int_0^T |y_s^{\varepsilon}||z_s^{\varepsilon}| \mathrm{d}s \right]^{\frac{q}{2}} \leq \left[\int_0^T \tfrac{1}{2}|y_s^{\varepsilon}|^2 + \tfrac{1}{2}|z_s^{\varepsilon}|^2 \mathrm{d}s \right]^{\frac{q}{2}}$$

$$\leq \left[\int_0^T |y_s^{\varepsilon}|^2 \mathrm{d}s \right]^{\frac{q}{2}} + \left[\int_0^T |z_s^{\varepsilon}|^2 \mathrm{d}s \right]^{\frac{q}{2}} \leq \int_0^T (|y_s^{\varepsilon}|^q + |z_s^{\varepsilon}|^q) \mathrm{d}s.$$

Taking expectation with $\mathbb{Q}$ on both hand sides gives us the claim. $\qquad\square$

3.3 Intuition: fast-wave averaging

Underneath the forthcoming proof lies a simple idea: for a complex valued process with constant fast angular rotation on the complex plane, e.g. $\exp(\mathrm{i}\varepsilon^{-1}t)$, its integral is of an order reciprocal to its angular speed, say ε. Moreover, for any fixed C^1 process $f(t)$, the time integral of its product with $\exp(\mathrm{i}\varepsilon^{-1}t)$ is or order ε as well, using the following integration by parts formula:

$$\int_0^T f(t) \exp(\mathrm{i}\varepsilon^{-1}t)\mathrm{d}t = \mathrm{i}\varepsilon \left[-\exp(\mathrm{i}\varepsilon^{-1}t)f(t)\Big|_0^T + \int_0^T \dot{f}(t)\exp(\mathrm{i}\varepsilon^{-1}t)\mathrm{d}t \right].$$

As a matter of fact, this Riemann-Lebesgue lemma type of argument was also used in the classical deterministic shallow water equation to explain the mode reduction in the singular limit. In [12, 14, 15], it is shown that the velocity field can be decomposed as $\vec{v}_t = \vec{v}_t^B + \exp(-\mathrm{i}t/\varepsilon)\vec{w}_t + o(1)$ as $\varepsilon \to 0$, where the first and second term represent the GB modes and gravity modes.

In our context, the gravity modes are evidently fast rotating. Looking back at their dynamics (1.2), $\hat{v}_{\mathbf{k}}$ has roughly an angular speed $\omega_{\mathbf{k}}$, which is of order ε^{-1}. What is left to

prove for our theorems is two fold: to show gravity waves' contribution to other elements in the filter, say the full filter's GB part, comes from integrated equations; we also need to construct a Riemann-Lebesgue lemma type of argument for stochastic processes under the setting of Section 3.2. The first objective is done by writing down the equations (2.14)-(2.20) in the fashion that $\mathbf{U}_s^g$ are shown explicitly. This will be carried out in detail during the proofs of Theorem 3.3 and 3.4. The second objective is fulfilled by the following two lemmas:

Lemma 3.6. *Let x_t^ε be a family of d-dimensional processes under a probability measure $\mathbb{Q}$ with dynamics:*

$$\mathrm{d}x_t^\varepsilon = (A_t^\varepsilon + \mathrm{i}\Omega_\varepsilon)x_t^\varepsilon \mathrm{d}t + b_t^\varepsilon \mathrm{d}t + D_t^\varepsilon \mathrm{d}W_t.$$

If $\{A_{t\leq T}^\varepsilon\}$ is ε-uniformly $\mathbb{Q}$-a.s. bounded, and $\{x_0^\varepsilon\}, \{b_{t\leq T}^\varepsilon\}, \{D_{t\leq T}^\varepsilon\}$ are ε-uniformly bounded in L^{2q} under $\mathbb{Q}$ for a $q \geq 1$, while Ω_ε is a real diagonal matrix, then $\{x_{t\leq T}^\varepsilon\}$ is ε-uniformly bounded in L_C^{2q} under $\mathbb{Q}$.

Proof. Let $y_t^\varepsilon = \exp(-\mathrm{i}\Omega_\varepsilon t)x_t^\varepsilon$, then by Itô's formula, y_t^ε solves:

$$\mathrm{d}y_t^\varepsilon = [\exp(-\mathrm{i}\Omega_\varepsilon t)A_t^\varepsilon \exp(\mathrm{i}\Omega_\varepsilon t)]y_t^\varepsilon \mathrm{d}t + \exp(-\mathrm{i}\Omega_\varepsilon t)b_t^\varepsilon \mathrm{d}t + (\exp(-\mathrm{i}\Omega_\varepsilon t)D_t^\varepsilon)\mathrm{d}W_t.$$

This can be seen as a diffusion process. Notice that $\|\exp(\pm\mathrm{i}\Omega_\varepsilon t)\| = 1$, we can simply apply Theorem 2.4.9 of [27] with $\tilde{x}_t \equiv 0$, which yields

$$\mathbb{E}\sup_{t\leq T}|x_t^\varepsilon|^{2q} = \mathbb{E}\sup_{t\leq T}|y_t^\varepsilon|^{2q} \leq N(q,A,T)(\|x_0^\varepsilon\|_{L^{2q}}^{2q} + \|b_{t\leq T}^\varepsilon\|_{L^{2q}}^{2q} + \|D_{t\leq T}^\varepsilon\|_{L^{2q}}^{2q})$$

with a function N. Here A is a constant such that $\|A_t^\varepsilon\| \leq A$ a.s. for all $t \leq T$. $\qquad\square$

Lemma 3.7. *Consider a family of d-dimensional processes under a probability measure $\mathbb{Q}$ with dynamics:*

$$\mathrm{d}x_t^\varepsilon = (A_t^\varepsilon + \mathrm{i}\Omega_\varepsilon)x_t^\varepsilon \mathrm{d}t + b_t^\varepsilon \mathrm{d}t + D_t^\varepsilon \mathrm{d}W_t.$$

Assume all the conditions in Lemma 3.6 hold and $\varepsilon\Omega_\varepsilon$ has a non singular limit for $\varepsilon \to 0$, then the following two hold:

(i) *Suppose $q \geq 2$, and there is a family of processes*

$$c_t^\varepsilon = c_0^\varepsilon + \int_0^t h_s^\varepsilon \mathrm{d}s + \int_0^t H_s^\varepsilon \mathrm{d}W_s,$$

with $\{c_0^\varepsilon\}, \{h_{t\leq T}^\varepsilon\}$ and $\{H_{t\leq T}^\varepsilon\}$ being ε-uniformly bounded in L^{2q} under $\mathbb{Q}$, then the process $z_s^\varepsilon := \int_0^s c_r^{\varepsilon*} x_r^\varepsilon \mathrm{d}r$ is of order ε in L_C^q under $\mathbb{Q}$.

(ii) *Assume moreover that $A_t^\varepsilon \equiv A^\varepsilon, D_t^\varepsilon \equiv 0$ and $x_0^\varepsilon = 0$, while the drift b_t^ε follows the dynamics:*

$$\mathrm{d}b_t^\varepsilon = \psi_t^\varepsilon \mathrm{d}t + \Psi_t^\varepsilon \mathrm{d}W_t$$

with $\{\psi_{t\leq T}^\varepsilon\}$ being ε-uniformly bounded in L^{2q} under $\mathbb{Q}$ and $\{\Psi_{t\leq T}^\varepsilon\}$ being ε-uniformly a.s. bounded, then $\{x_{t\leq T}^\varepsilon\}$ is of order ε in L_C^{2q} under $\mathbb{Q}$.

Remark 3.8. *Our problem can also be interpreted in the classical multi-scale analysis setting, as the complex argument of the gravity modes are fast processes while the GB modes and the modulus of the gravity modes are slow processes. Yet, as the filter equations involve multiple processes, the classical multi-scale decomposition analysis is more cumbersome than the direct approach through Lemma 3.7.*

Proof. Since there is only one measure $\mathbb{Q}$ in this lemma, we will omit its appearance.

Part (i) Denote $f_t^\varepsilon = A_t^\varepsilon x_t^\varepsilon + b_t^\varepsilon$, by Lemma 3.6 and Hölder's inequality, $\{f_{t\leq T}^\varepsilon\}$ is ε-uniformly bounded in L^{2q}. Denote the jth diagonal entry of Ω_ε as w_j^ε, then the jth component of x_t^ε is the solution to

$$d(x_t^\varepsilon)_j = i\omega_j^\varepsilon (x_t^\varepsilon)_j dt + [f_t^\varepsilon dt + D_t^\varepsilon dW_t]_j,$$

here and after $(\ )_j$ denotes the jth component of a vector. Hence $(x_t^\varepsilon)_j$ can be written as

$$(x_t^\varepsilon)_j = \exp(i\omega_j^\varepsilon t)(x_0^\varepsilon)_j + \int_0^t \exp(i\omega_j^\varepsilon(t-s))[f_s^\varepsilon ds + D_s^\varepsilon dW_s]_j. \tag{3.1}$$

Therefore if we denote $g_t^\varepsilon = \int_0^t x_s^\varepsilon ds$, g_t^ε is progressively measurable with the following formulation using Fubini's theorem for stochastic integral [28]:

$$\varepsilon^{-1} g_t^\varepsilon = \frac{1}{i\varepsilon\omega_j^\varepsilon}\left[(\exp(i\omega_j^\varepsilon t) - 1)(x_0^\varepsilon)_j + \int_0^t (\exp(i\omega_j^\varepsilon(t-s)) - 1)[f_s^\varepsilon ds + D_s^\varepsilon dW_s]_j\right]. \tag{3.2}$$

Notice that, first, $|\exp(i\omega_j^\varepsilon s)| \leq 1$ and $\varepsilon\omega_j^\varepsilon$ are both ε-uniformly bounded; second the process

$$\phi_t^\varepsilon := \int_0^t (\exp(i\omega_j^\varepsilon(t-s)) - 1)[f_s^\varepsilon ds + D_s^\varepsilon dW_s]_j$$

is an Itô process with terms ε-uniformly bounded in L^{2q}, so by Lemma 3.6, $\{\phi_{t\leq T}^\varepsilon\}$ is ε-uniformly bounded in L_C^{2q}. So in the view of (3.2), $\{g_{t\leq T}^\varepsilon\}$ is of order ε in L_C^{2q}.

Apply the integration by parts formula for stochastic integrals to z_t^ε, we have

$$\varepsilon^{-1} z_t^\varepsilon = c_t^{\varepsilon*}(\varepsilon^{-1} g_t^\varepsilon) - \int_0^t h_s^{\varepsilon*}(\varepsilon^{-1} g_s^\varepsilon)ds - \int_0^t [(\varepsilon^{-1} g_s^{\varepsilon*})H_s^{\varepsilon*} dW_s]^*.$$

Using Lemma 3.6 and the conditions in this lemma, $\{c_{t\leq T}^\varepsilon\}$ is ε-uniformly bounded in L_C^{2q}. Hence $c_s^{\varepsilon*}(\varepsilon^{-1} g_s^\varepsilon)$ is ε-uniformly bounded in L_C^q. Moreover,

$$\tilde{w}_t^\varepsilon := \int_0^t h_s^{\varepsilon*}(\varepsilon^{-1} g_s^\varepsilon)ds + \int_0^t [(\varepsilon^{-1} g_s^{\varepsilon*})H_s^{\varepsilon*} dW_s]^*$$

is an Itô process with terms ε-uniformly bounded in L^q, so by Lemma 3.6, $\{\tilde{w}_{t\leq T}^\varepsilon\}$ is ε-uniformly bounded in L_C^q. As a consequence, $\{z_{t\leq T}^\varepsilon\}$ is of order ε in L_C^q.

Part (ii) With $x_0^\varepsilon, D_t^\varepsilon = 0$, (3.1) becomes: $(x_t^\varepsilon)_j = \int_0^t \exp(i\omega_j^\varepsilon(t-s))(f_s^\varepsilon)_j ds$. Apply Itô's formula to $f_t^\varepsilon = A^\varepsilon x_t^\varepsilon + b_t^\varepsilon$,

$$df_t^\varepsilon = [A^\varepsilon[(A^\varepsilon + i\Omega_\varepsilon)x_t^\varepsilon + b_t^\varepsilon] + \psi_t^\varepsilon]dt + \Psi_t^\varepsilon dW_t.$$

Denote $u_t^\varepsilon = A^\varepsilon[(A^\varepsilon + i\Omega_\varepsilon)x_t^\varepsilon + b_t^\varepsilon] + \psi_t^\varepsilon$, according to Lemma 3.6, it is ε-uniformly bounded in L^{2q}. Consider the following integration by part formula applied to (3.1):

$$\varepsilon^{-1}(x_t^\varepsilon)_j = \varepsilon^{-1}\int_0^t \exp(i\omega_j^\varepsilon(t-s))(f_s^\varepsilon)_j ds$$

$$= \frac{\exp(i\omega_j^\varepsilon t)}{i\omega_j^\varepsilon \varepsilon}\left[(f_0^\varepsilon)_j(1 - \exp(-i\omega_j^\varepsilon t)) - \int_0^t (1 - \exp(-i\omega_j^\varepsilon s))(u_s^\varepsilon ds + \Psi_s^\varepsilon dW_s)_j\right].$$

The integral process $\int_0^t (1 - e^{-i\omega_j^\varepsilon s})(u_s^\varepsilon ds + H_s^\varepsilon dW_s)_j$ fits the conditions of Lemma 3.6, hence $\{x_{t\leq T}^\varepsilon\}$ is of order ε in L_C^{2q}. $\qquad\square$

14

4 Proofs for the theorems

4.1 Limiting reduced filter behavior

Proof of Theorem 3.3. We will only prove the statements under $\mathbb{P}$, hence we do not mention $\mathbb{P}$ explicitly. The proof for the case of $\mathbb{P}_{\vec{v}^B}$ is identical. To see this it suffices to single out the process $\mathbf{U}_t^B$ in our proof, which under $\mathbb{P}_{\vec{v}^B}$ is a deterministic bounded process for a.e. realization of $\vec{v}_{t\geq 0}^B$.

In order to analyze the GB part and gravity part of the vector and matrix processes, we use the following notation:

$$R_t = \begin{bmatrix} R_t^B, & S_t \\ S_t^*, & R_t^g \end{bmatrix}, \quad \mathbf{P}_t = \begin{bmatrix} \mathbf{P}_X^{v*}(\mathbf{X}_t)\mathbf{P}_X^B(\mathbf{X}_t) & \mathbf{P}_X^{v*}(\mathbf{X}_t)\mathbf{P}_X^g(\mathbf{X}_t) \\ \mathbf{P}_X^{g*}(\mathbf{X}_t)\mathbf{P}_X^B(\mathbf{X}_t) & \mathbf{P}_X^{g*}(\mathbf{X}_t)\mathbf{P}_X^g(\mathbf{X}_t) \end{bmatrix} := \begin{bmatrix} \mathbf{P}_t^B & Q_t \\ Q_t^* & \mathbf{P}_t^g \end{bmatrix},$$

one can check explicitly that entry-wise $(\mathbf{P}_t)_{\mathbf{j},\mathbf{k}} = \sum_{l=1}^{L} \exp(\mathrm{i}(\vec{k} - \vec{j}) \cdot \vec{X}_l(t))(\vec{r}_j^* \vec{r}_{\mathbf{k}})$.

$$\Gamma = \begin{bmatrix} \Gamma^B & 0 \\ 0 & \Gamma^g - \Omega_\varepsilon i \end{bmatrix}, \quad \Omega_\varepsilon = \begin{bmatrix} \ddots & & \\ & \omega_{\mathbf{k}} & \\ & & \ddots \end{bmatrix}, \quad \mathbf{\Sigma} = \Sigma_u \Sigma_u^* = \begin{bmatrix} \Sigma_u^{B*}\Sigma_u^B & 0 \\ 0 & \Sigma_u^{g*}\Sigma_u^g \end{bmatrix} = \begin{bmatrix} \mathbf{\Sigma}^B & 0 \\ 0 & \mathbf{\Sigma}^g \end{bmatrix}.$$

Part (i) First of all, $\mathbf{P}_t$, $\mathbf{P}_X(\mathbf{X}_t)$ and their sub-matrices are all ε-uniformly a.s. bounded, since these matrices have entries bounded by either L or 1 in norm. Next we show $\{R_{t\leq T}\}$ is ε-uniformly a.s. bounded. This can be done by seeing R_t is the solution to the Riccati equation (2.15). By the comparison theorem, Theorem 4.1.4 [29], R_t will be bounded above in the Hermitian sense by the solution of the following:

$$\mathrm{d}U_t = [-\Gamma U_t - U_t \Gamma^* + \mathbf{\Sigma}]\mathrm{d}t.$$

As this equation is diagonalizable, and $\|\exp(-\Gamma s)\|$ is ε-uniformly bounded for $t \leq T$, one can easily find an ε-uniform upper bound for R_t. Therefore as sub-matrices, R_t^B, R_t^g are also ε-uniformly a.s. bounded. A similar ε-uniformly a.s. upper bound can be found for $\|R_t^r\|$.

Next, we will show the off-diagonal term of R_t, denoted by S_t in (2.16), is of order ε in L_C^{2q}. Rewrite the differential Riccati equation (2.15) in sub-matrices form:

$$\mathrm{d}R_t = \begin{bmatrix} -2\Gamma^B R_t^B + \mathbf{\Sigma}^B & [-2\overline{\Gamma} + \mathrm{i}\Omega_\varepsilon]S_t \\ [-2\overline{\Gamma} - \mathrm{i}\Omega_\varepsilon]S_t^* & -2\Gamma^G R_t^g + \mathbf{\Sigma}^G \end{bmatrix} \mathrm{d}t - \sigma_x^{-2} R_t \mathbf{P}_t R_t \mathrm{d}t, \quad 2\overline{\Gamma} := \Gamma^B + \Gamma^G. \quad (4.1)$$

Take out the $(\mathbf{K}_B, \mathbf{K}_g)$th sub-matrix, which is the evolution for S_t:

$$\mathrm{d}S_t = [-2\overline{\Gamma} + \mathrm{i}\Omega_\varepsilon]S_t \mathrm{d}t - \sigma_x^{-2}[R_t \mathbf{P}_t R_t]_{\mathbf{K}_B, \mathbf{K}_g} \mathrm{d}t.$$

Here we use $[A]_{\mathbf{K}_B, \mathbf{K}_g}$ to denote the $(\mathbf{K}_B, \mathbf{K}_g)$th sub-matrix of a matrix A. In order to apply Lemma 3.7 (ii) on S_t, it suffices to consider each column of S_t, i.e. with index $\mathbf{k} \in \mathbf{K}_g$,

$$[\dot{S}_t]_{\mathbf{K}_B,\mathbf{k}} = [-2\overline{\Gamma} + \mathrm{i}\Omega_\varepsilon][S_t]_{\mathbf{K}_B,\mathbf{k}} - \sigma_x^{-2}[R_t \mathbf{P}_t R_t]_{\mathbf{K}_B,\mathbf{k}}.$$

The time differential for the drift term is

$$\mathrm{d}R_t \mathbf{P}_t R_t = (\dot{R}_t \mathbf{P}_t R_t + R_t \mathbf{P}_t \dot{R}_t)\mathrm{d}t + R_t \mathrm{d}\mathbf{P}_t R_t.$$

15

Using that $\mathbf{P}_t$ and R_t are both ε-uniformly a.s. bounded, $\dot{R}_t$,i.e. (2.15), as a continuous function of them is also ε-uniformly a.s. bounded. On the other hand as $\mathbf{P}_t$ depends smoothly on $\mathbf{X}_t$, so by applying the Itô formula, for each fixed $\mathbf{k} \in \mathbf{K}_g$ there are some proper b_t and Σ_t such that

$$d[R_t \mathbf{P}_t R_t]_{\mathbf{K}_B,\mathbf{k}} = b_t dt + \Sigma_t dW_t^x,$$

where $|b_t| \leq b(|\mathbf{U}_t^B| + |\mathbf{U}_t^g| + 1), \|\Sigma_t\| \leq b$ with ε-uniform b. As $\mathbf{U}_t^B$ and $\mathbf{U}_t^g$ satisfy the conditions of Lemma 3.6, they are ε-uniformly bounded in L_C^{2q}. Hence $[\dot{S}_t]_{\mathbf{K}_B,\mathbf{k}}$ qualifies for the application of Lemma 3.7 (ii). Therefore, S_t is of order ε in L_C^{2q}.

Next, we will study the evolution of R_t^B, the $(\mathbf{K}_B, \mathbf{K}_B)$ sub-block of (4.1), which can be written out explicitly:

$$dR_t^B = [-2\Gamma^B R_t^B + \mathbf{\Sigma}^B - \sigma_x^{-2} R_t^B \mathbf{P}_t^B R_t^B - \sigma_x^{-2}(S_t Q_t^* R_t^B + R_t^B Q_t^* S_t^* + S_t \mathbf{P}_t^B S_t^*)]dt$$
$$= [-2\Gamma^B R_t^B + \mathbf{\Sigma}^B - \sigma_x^{-2} R_t^B \mathbf{P}_t^B R_t^B - \sigma_x^{-2} L_t]dt$$

with L_t being the sum in the bracket of the first line. Notice that $\{R_{t \leq T}\}, \{\mathbf{P}_{t \leq T}\}$ are both ε-uniformly a.s. bounded, $\{L_{t \leq T}\}$ is of order ε in L_C^{2q} since $\{S_{t \leq T}\}$ is. Hence R_t^B can be seen as a solution of (2.20) with a perturbation $L_{t \leq T}$, as $\mathbf{P}_t^B = \mathbf{P}_X^{B*}(\mathbf{X}_t)\mathbf{P}_X^B(\mathbf{X}_t)$. For this purpose, we apply the result of [30], where it is shown that if $\delta \leq (4\nu^2 pS)^{-1}$ then $\Delta R_t = R_t^B - R_t^r$ is bounded by

$$\|\Delta R_t\| \leq \frac{2\nu p\delta}{1 + \sqrt{1 - 4\nu^2 pS\delta}} \quad \text{a.s.} \quad \forall t \leq T,$$

with the constants given by

$$\nu = \max_{t \leq T}\left\{\int_0^t \|\Phi(s,t)\| ds\right\}, \quad p = \sup_{t \leq T}\|R_t^r\|, \quad S = \sup_{t \leq T}\|\mathbf{P}_t^B\|, \quad \delta = \sigma_x^{-2}\sup_{t \leq T}\|L_t\|.$$
$$(4.2)$$

Here Φ is the fundamental matrix generated by $-\Gamma^B - \sigma_x^{-1}\mathbf{P}_s R_s^r$, which is also ε-uniformly a.s. bounded. Notice that ν, p, S are all ε-uniformly bounded, hence if we write the a.s. upper bound of $\|R_s^B\|, \|R_s^r\|$ as A, then by the Markov inequality

$$\mathbb{E}\sup_{t \leq T}\|\Delta R_t\|^{2q} = \mathbb{E}\sup_{t \leq T}\|\Delta R_t\|^{2q}1_{\{\delta \geq (4\nu^2 pS)^{-1}\}} + \mathbb{E}\sup_{t \leq T}\|\Delta R_t\|^{2q}1_{\{\delta < (4\nu^2 pS)^{-1}\}}$$
$$\leq 2A\mathbb{P}(\delta \geq (4\nu^2 pS)^{-1}) + 4^q\nu^{2q}p^{2q}\mathbb{E}\delta^{2q}$$
$$\leq 2^{2q+1}A\nu^{4q}p^{2q}S^{2q}\mathbb{E}\delta^{2q} + 4^q\nu^{2q}p^{2q}\mathbb{E}\delta^{2q}.$$
$$(4.3)$$

Since $\mathbb{E}\delta^{2q} = \sigma_x^{-4q}\|L_{t \leq T}\|_{L_C^{2q}}^{2q}$, it is of order ε^{2q}. Hence $\{\Delta R_{t \leq T}\}$ is also of order ε in L_C^{2q}.

Part (ii) Recall that $d\mathbf{X}_t = \mathbf{P}_X(\mathbf{X}_t)\mathbf{U}_t dt + \sigma_x dW_t^x$, we can expand the posterior mean dynamics (2.19) and (2.14)'s GB part, and rewrite them in the following fashion:

$$dm_t^r = (-2\Gamma^B m_t^r + F_t^B)dt + \sigma_x^{-2} R_t^r \mathbf{P}_X^{B*}(\mathbf{X}_t)[d\mathbf{X}_t - \mathbf{P}_X^B(\mathbf{X}_t)m_t^r dt]$$
$$= (-2\Gamma^B - \sigma_x^{-2} R_t^r \mathbf{P}_t^B)m_t^r dt + [F_t^B + \sigma_x^{-2} R_t^r \mathbf{P}_X^{B*}(\mathbf{X}_t)\mathbf{P}_X(\mathbf{X}_t)\mathbf{U}_t]dt + \sigma_x^{-1} R_t^r \mathbf{P}_X^{B*}(\mathbf{X}_t)dW_t^x$$
$$= A_t^r m_t^r dt + C_t^r dt + D_t^r dW_t^x.$$
$$(4.4)$$

And the GB component of the full filter follows:

$$\begin{aligned}
\mathrm{d}m_t^B &= (-2\Gamma^B m_t^B + F_t^B)\mathrm{d}t + \sigma_x^{-2}(R_t^B \mathbf{P}_X^{B*}(\mathbf{X}_t) + S_t \mathbf{P}_X^{g*}(\mathbf{X}_t))\mathrm{d}\mathbf{X}_t - \sigma_x^{-2}(R_t^B \mathbf{P}_t^B + S_t Q_t^*)m_t^B \mathrm{d}t \\
&\quad - \sigma_x^{-2}(R_t^B Q_t + S_t \mathbf{P}_t^g)m_t^g \mathrm{d}t \\
&= (-2\Gamma^B - \sigma_x^{-2}(R_t^B \mathbf{P}_t^B + S_t Q_t^*))m_t^B \mathrm{d}t - \sigma_x^{-2}(R_t^B Q_t + S_t \mathbf{P}_t^g)m_t^g \mathrm{d}t \\
&\quad + (F_t^B + \sigma_x^{-2}(R_t^B \mathbf{P}_X^{B*}(\mathbf{X}_t) + S_t \mathbf{P}_X^{g*}(\mathbf{X}_t))\mathbf{P}_X(\mathbf{X}_t)\mathbf{U}_t)\mathrm{d}t + \sigma_x^{-1} R_t^B \mathbf{P}_X^{B*}(\mathbf{X}_t)\mathrm{d}W_t^x \\
&= A_t^B m_t^B \mathrm{d}t + B_t^B m_t^g \mathrm{d}t + C_t^B \mathrm{d}t + D_t^B \mathrm{d}W_t^x \qquad\qquad (4.5)
\end{aligned}$$

The H_t^B and $H_t^r, H = A, B, C, D$, are defined by their previous lines in an obvious way. It is important to notice that $\{H_{t\leq T}^B\}$ and $\{H_{t\leq T}^r\}$ are ε-uniformly a.s. bounded for $H = A, B, D$ and in L^{2q} for $H = C$. If we denote $\Delta H_t = H_t^B - H_t^r$, then

$$\Delta A_t = -\sigma_x^{-2}[(\Delta R_t)\mathbf{P}_t^B + S_t Q_t^*], \quad \Delta D_t = \sigma_x^{-1}(\Delta R_t)\mathbf{P}_X^{B*}(\mathbf{X}_t),$$

are both of order ε in L_C^{2q} by part (i). Likewise

$$\Delta C_t = [(\Delta R_t)\mathbf{P}_X^{B*}(\mathbf{X}_t) + S_t \mathbf{P}_X^{g*}(\mathbf{X}_t)]\mathbf{P}_X(\mathbf{X}_t)\mathbf{U}_t$$

is of order ε in L^q by part (i).

Let $\Psi^B(s,t), \Psi^r(s,t)$ be the fundamental matrice generated by A_t^B and A_t^r respectively. Evidently they are both ε-uniformly a.s. bounded. Next we show that $\sup_{s\leq t\leq T}\|\Delta\Psi(s,t)\|$ is of order ε in L^{2q}. To do this, consider two processes

$$x_t^B = \Psi^B(s,t)x_s, \quad x_t^r = \Psi^r(s,t)x_s, \quad |x_s| = 1;$$

and their difference $y_t = x_t^B - x_t^r = \Delta\Psi(s,t)x_s$. They are all ε-uniformly bounded processes. Moreover, the differential form of y_t is $\mathrm{d}y_t = A_t^B y_t \mathrm{d}t + (A_t^B - A_t^r)x_t^r \mathrm{d}t$. We can establish the following bound using Grönwall's inequality,

$$|y_t| \leq \int_s^t \|\Psi^B(u,t)\|\|A_u^B - A_u^r\||x_u^r|du \quad a.s.$$

As $\Psi^B(u,s)$ and x_u^r are both ε-uniformly a.s. bounded, and $\{\Delta A_{t\leq T}\}$ is of oder ε in L_C^{2q}, one can establish an ε-uniform a.s. bound for $|y_t|$ with different choice of $s \leq t \leq T$. Since $\|\Delta\Psi(s,t)\| = \sup_{|x_s|\leq 1}|y_s|$, $\sup_{s\leq t\leq T}\|\Delta\Psi(s,t)\|$ is of order ε in L^{2q}.

Now go back to m_t^B and m_t^r, they can be written out as:

$$m_t^B = \Psi^B(0,t)m_0^B + \int_0^t \Psi^B(s,t)B_s^B m_s^g \mathrm{d}s + \int_0^t \Psi^B(s,t)[C_s^B \mathrm{d}s + D_s^B \mathrm{d}W_s^x],$$

$$m_t^r = \Psi^r(0,t)m_0^r + \int_0^t \Psi^r(s,t)[C_s^r \mathrm{d}s + D_s^r \mathrm{d}W_s^x].$$

The difference between the two is:

$$\Delta\Psi(0,t)m_0^B + \int_0^t \Psi^B(s,t)B_s^B m_s^g \mathrm{d}s + \int_0^t \Delta(\Psi(s,t)C_s)\mathrm{d}s + \int_0^t \Delta(\Psi(s,t)D_s)\mathrm{d}W_s^x. \quad (4.6)$$

From the previous derivation, the first term above, $\Delta\Psi(0,t)m_0^B$ is of order ε in L_C^{2q}. The third term,

$$\int_0^t \Delta(\Psi(s,t)C_s)\mathrm{d}s = \int_0^t (\Delta\Psi(s,t))C_s^B \mathrm{d}s + \int_0^t \Psi^r(s,t)(\Delta C_s)\mathrm{d}s,$$

17

as a process, is of order ε in L_C^q. Likewise, the fourth term in (4.6) is

$$\int_0^t \Delta(\Psi(s,t)D_s)\mathrm{d}W_s^x = \int_0^t (\Delta\Psi(s,t))D_s^B\mathrm{d}W_s^x + \int_0^t \Psi^r(s,t)(\Delta D_s)\mathrm{d}W_s^x$$

as a process, is of order ε in L_C^q.

So it remains to show the second term in (4.6), $\int_0^t \Psi^B(s,t)B_s^B m_s^g \mathrm{d}s$, is of order ε in L_C^q. It suffices to check the conditions of Lemma 3.7, part (i). First, using the gravity part of (2.14), which alternates superscripts g and B in (4.5), we rewrite $\mathrm{d}m_t^g$ in the following fashion:

$$\mathrm{d}m_t^g = [A_t^g + \mathrm{i}\Omega_\varepsilon]m_t^g \mathrm{d}t + B_t^g m_t^B \mathrm{d}t + C_t^g \mathrm{d}t + D_t^g \mathrm{d}W_t^x$$

where A_t^g, D_t^g are ε-uniformly bounded a.s and $B_t^g m_t^B, C_t^g$ are ε-uniformly bounded in L_C^{2q}. This qualifies m_t^g as a fast rotational process. Next, recall that

$$B_t^B = -\sigma_x^{-2}(R_t^B Q_t + S_t P_t^g);$$

applying the Itô's formula, one can verify that for each row of B_t^B, i.e. each column of B_t^{B*}, there are processes b_t, Σ_t such that:

$$\mathrm{d}[B_t^{B*}]_{\mathbf{K}_g,\mathbf{k}} = b_t \mathrm{d}t + \Sigma_t \mathrm{d}W_t^{x*}, \quad \mathbf{k} \in \mathbf{K}_g$$

with $|b_t| \leq b(|\mathbf{U}_t| + 1), |\Sigma_t| \leq b$ a.s. for some ε-uniform b. So each row of B_t^B, and hence also B_t^B, qualify as the c_t^ε integrating process in Lemma 3.7, part (i). Therefore, $M_t := \int_0^t B_s^B m_s^g \mathrm{d}s$ is of order ε in L_C^q. Apply the integration by part formula:

$$\int_0^t \Psi^B(s,t)B_s^B m_s^g \mathrm{d}s = M_t - \int_0^t \Psi^B(s,t)A_s^B M_s \mathrm{d}s.$$

Notice that $\Psi^B(s,t)$ and A_s^B are ε-uniformly a.s. bounded, $\int_0^t \Psi^B(s,t)B_s^B m_s^g \mathrm{d}s$ as a process is of order ε in L_C^q. $\qquad\square$

Remark 4.1. *If one carefully follow the σ_x's appearance in various perturbations, one finds it comes as a coefficient of form σ_x^{-2}. In a sense, this indicates that small σ_x leads to larger deviation between different filters, which will be shown in numerical experiments by Figure 5.6 in Section 5. Likewise, the number of L also increases the difference through the term $\mathbf{P}_t$ on average.*

4.2 Limiting tracer trajectory

Before we proceed to the proof of Theorem 3.4, we must study the trajectory of tracers in full flow, $\vec{X}_l(t)$, and in GB flow, $\vec{X}_l^B(t)$, as they are the input for the full filter and GB filter respectively. Interestingly, they are close to each other for small Rossby number, because the contribution of gravity waves to the tracers' dislocation comes in an integral fashion. Thus, for small ε, the difference of the two trajectories is of order ε for a bounded time interval. More precisely, we have the following:

Proposition 4.2. *Fix any fixed $T > 0, q > 1$, consider a noisy Lagrangian tracer $\vec{X}_l(t)$ driven by the full flow $\vec{v}_t$ and a noisy Lagrangian tracer $\vec{X}_l^B(t)$ driven by the GB part $\vec{v}_t^B$. Assume the stochastic noises $W_l^x(s)$ in (1.3) and (1.4) that drive both tracers are identical. Then the difference of two tracers' location $y_t := \vec{X}_l(s) - \vec{X}_l^B(t), t \leq T$ is of order ε in L_C^q under $\mathbb{P}_{\vec{v}^B}$ for a.s. realization of $\vec{v}_{t\geq 0}^B$.*

Proof. With any velocity field $\vec{u}_{t \leq T}$, denote

$$|\vec{u}|_{1,\infty} := \sup_{t \leq T, \vec{x}} |\vec{u}(\vec{x}, t)| \vee |\partial_{\vec{x}} \vec{u}(\vec{x}, t)|.$$

First note that according to (1.3) y_t is the solution to the following:

$$\dot{y}_t = \vec{v}^B(y_t + \vec{X}_l^B(t), t) - \vec{v}^B(\vec{X}_l^B(t), t) + \vec{v}^g(\vec{X}_l(t), t), \quad y_0 = 0.$$

Therefore $|\dot{y}_t| \leq 2|\vec{v}^B|_{1,\infty} + |\vec{v}^g|_{1,\infty}$. As $\vec{v}^g(\vec{x}) = P_X(\vec{x})\mathbf{U}_s^g$ and $\mathbf{U}_s^g$ is ε-uniformly bounded in L_C^{2q} by Lemma 3.6, so $y_{t \leq T}$ and $|\dot{y}_{t \leq T}|$ are both ε-uniformly bounded in L_C^{2q} under $\mathbb{P}_{\vec{v}^B}$ for a.s. realization of $\vec{v}_{t \geq 0}^B$. Using the bound $|\vec{v}^B(y_t + \vec{X}_l^B(t), t) - \vec{v}^B(\vec{X}_l^B(t), t)| \leq |\vec{v}^B|_{1,\infty}|y_t|$ and the formula of $\dot{y}_t$, one has

$$|y_t| \leq \left| \int_0^t \vec{v}^g(\vec{X}_l(s), s)\mathrm{d}s \right| + \left| \int_0^t (\vec{v}^B(y_s + \vec{X}_l^B(s), s) - \vec{v}^B(\vec{X}_l^B(s), s))\mathrm{d}s \right|$$

$$\leq \left| \int_0^t \vec{v}^g(\vec{X}_l(s), s)\mathrm{d}s \right| + \int_0^t |\vec{v}^B|_{1,\infty}|y_s|\mathrm{d}s$$

Using the integral form of Grönwall's inequality, one can conclude that:

$$|y_t| \leq \left| \int_0^t \vec{v}^g(\vec{X}_l(r), r)\mathrm{d}r \right| + \int_0^t \left| \int_0^s \vec{v}^g(\vec{X}_l(r), r)\mathrm{d}r \right| |\vec{v}^B|_{1,\infty} \exp(|\vec{v}^B|_{1,\infty}(t - s))\mathrm{d}s$$

$$\leq \left[1 + \exp(|\vec{v}^B|_{1,\infty}t) \right] \sup_{t \leq T} \left| \int_0^t \vec{v}^g(\vec{X}_l(r), r)\mathrm{d}r \right|. \tag{4.7}$$

Since $|\vec{v}^B|_{1,\infty}$ is a deterministic constant under $\mathbb{P}_{\vec{v}^B}$, it suffices to show $\int_0^t \vec{v}^g(\vec{X}_l(r), r)dr$ is of order ε in L_C^q to prove this proposition. Next notice that

$$\int_0^t \vec{v}^g(\vec{X}_l(s), s)\mathrm{d}s = \sum_{\mathbf{k} \in \mathbf{K}_g} \vec{r}_{\mathbf{k}} \int_0^t \exp(i\vec{k} \cdot \vec{X}_l(s))\hat{v}_{\mathbf{k}}(s)\mathrm{d}s.$$

For each gravity mode $\mathbf{k} \in \mathbf{K}_g$, $\hat{v}_{\mathbf{k}}$ is a fast rotational process based on its dynamics (2.9); on the other hand by Itô's formula, $\exp(i\vec{k} \cdot \vec{X}_l(s))$ has its differential as:

$$\mathrm{d}\exp(i\vec{k} \cdot \vec{X}_l(s)) = \exp(i\vec{k} \cdot \vec{X}_l(s))[i\vec{k} \cdot \vec{v}(\vec{X}_l(s), s) - |\vec{k}|^2\sigma_x^2]\mathrm{d}s + i\exp(i\vec{k} \cdot \vec{X}_l(s))\vec{k} \cdot \sigma_x\mathrm{d}W_l^x(s).$$

Using Lemma 3.6, it is elementary to check that each terms above is ε-uniformly bounded in L^q under $\mathbb{P}_{\vec{v}^B}$. According to Lemma 3.6 (i), $\int_0^t \exp(i\vec{k} \cdot \vec{X}_l(s))\hat{v}_{\mathbf{k}}(s)\mathrm{d}s$ hence also $\int_0^t \vec{v}^g(\vec{X}_l(s), s)\mathrm{d}s$ are of order ε in L_C^q under $\mathbb{P}_{\vec{v}^B}$. $\square$

Remark 4.3. *Judging from (4.7), one sees the reason why $\mathbb{P}_{\vec{v}^B}$ instead of $\mathbb{P}$ must be applied here, because the expectation of (4.7) might not be finite. This also implies that in practice this proposition is hard to be validated in numerics for large T.*

Remark 4.4. *Since $\vec{X}_l^B(s)$ are driven by incompressible flows, by Theorem 3.1 of [8] the invariant distribution for their projection over the periodic domain $\mathbb{T}^2 = (-\pi, \pi]^2$ is the uniform distribution. By Proposition 4.2, we know the distribution of $\vec{X}_l(s)$ is close to the uniform distribution for $\varepsilon \ll 1$ if they are distributed uniformly initially. This will be found numerically in Section 5 by comparing the configurations of tracers in Figure 5.2 for different ε.*

19

4.3 GB Filter as an approximation of the full filter

Proposition 4.2 indicates that trajectories observed by the GB filter and the full filter are close to each other for order one times and small ε. Armed with this result, the proof of Theorem 3.4 is rather similar to the one of Theorem 3.3.

Proof of Theorem 3.4. By Theorem 3.3, it suffices to show that $R_s^r - R_s^G, m_s^r - m_s^G$ are processes of order ε in L_C^{2q} or L_C^q in $\mathbb{P}_{\vec{v}^B}$ for a.s. realization of $\vec{v}_{t\geq 0}^B$. In other words, we are comparing the GB filter and the reduced filter instead. For this purpose, we will fix a realization of $\vec{v}_{t\geq 0}^B$ and discuss everything under $\mathbb{P}_{\vec{v}^B}$, of which the appearance will be omitted.

Part (i) First of all, we compare the evolution of R_t^G and R_t^r, (2.18) and (2.20), they share the same initial value and:

$$\dot{R}_t^r = -\Gamma^B R_t^r - R_t^r \Gamma^B + \mathbf{\Sigma}^B - \sigma_x^{-2} R_t^r \mathbf{P}_t^B R_t^r, \quad \dot{R}_t^G = -\Gamma^B R_t^G - R_t^G \Gamma^B + \mathbf{\Sigma}^B - \sigma_x^{-2} R_t^G \mathbf{P}_t^G R_t^G.$$

where $\mathbf{P}_t^B = \mathbf{P}_X^{B*}(\mathbf{X}_t)\mathbf{P}_X^B(\mathbf{X}_t)$ and $\mathbf{P}_t^G = \mathbf{P}_X^{B*}(\mathbf{X}_t^B)\mathbf{P}_X^B(\mathbf{X}_t^B)$. Notice that $\mathbf{P}_X^{B*}(\mathbf{X}_t)$ is a C^1 function of its variable and by Proposition 4.2, $|\mathbf{X}_s - \mathbf{X}_s^G|$ is of order ε in L_C^{2q}, hence is also the process $(\mathbf{P}_s^G - \mathbf{P}_s^B)$. Applying the sensitivity analysis of the Riccati equation [30], we have:

$$\|R_s^r - R_s^G\| \leq \frac{2\nu p\delta}{1 + \sqrt{1 - 4\nu^2 pS\delta}} \quad \mathbb{P}_{\vec{v}^B}\text{-a.s.} \quad \forall t \leq T,$$

with the same definition for ν, p, S as in (4.2) but $\delta = \sigma_x^{-2} \sup_{s\leq T} \|\mathbf{P}_s^G - \mathbf{P}_s^B\|$. Then as in (4.3), using δ being of order ε in L^{2q}, we can conclude $\|R_s^r - R_s^G\|$ is of order $\sqrt{\varepsilon}$ in L_C^{2q}.

Part (ii) Recall (4.4), which can be written into following fashion:

$$\begin{aligned}
dm_t^r &= (-\Gamma^B - \sigma_x^{-2} R_t^r \mathbf{P}_t^B)m_t^r dt + [F_t^B + \sigma_x^{-2} R_t^r \mathbf{P}_X^{B*}(\mathbf{X}_t)\mathbf{P}_X^B(\mathbf{X}_t)\mathbf{U}_t]dt + \sigma_x^{-1} R_t^r \mathbf{P}_X^{B*}(\mathbf{X}_t)dW_t^x \\
&= (-\Gamma^B - \sigma_x^{-2} R_t^r \mathbf{P}_t^B)m_t^r dt + [F_t^B + \sigma_x^{-2} R_t^r \mathbf{P}_t^B \mathbf{U}_t^B]dt + \sigma_x^2 R_t^r Q_t \mathbf{U}_t^g dt + \sigma_x^{-1} R_t^r \mathbf{P}_X^{B*}(\mathbf{X}_t)dW_t^x \\
&= A_t^r m_t^r dt + B_t^r \mathbf{U}_t^g dt + C_t^r dt + D_t^r dW_t^x.
\end{aligned}$$

For the GB filter, the evolution of m_t^G will be

$$\begin{aligned}
dm_t^G &= (-\Gamma^B m_t^G + F_t^B)dt + \sigma_x^{-2} R_t^G \mathbf{P}_X^{B*}(\mathbf{X}_t^B)d\mathbf{X}_t^B - \sigma_x^{-2} R_t^B \mathbf{P}_t^G m_t^G dt \\
&= (-\Gamma^B - \sigma_x^{-2} R_t^G \mathbf{P}_t^G)m_t^G dt + (F_t^B + \sigma_x^{-2} R_t^G \mathbf{P}_t^G \mathbf{U}_t^B)dt + \sigma_x^{-1} R_t^G \mathbf{P}_X^{B*}(\mathbf{X}_t^B)dW_t^x \\
&= A_t^G m_t^G dt + C_t^G dt + D_t^G dW_t^x.
\end{aligned}$$

It is important to notice that $\{H_{t\leq T}^G\}$ and $\{H_{t\leq T}^r\}$ are ε-uniformly a.s. bounded for $H = A, B, D$ and in L^{2q} for $H = C$. If we denote $\Delta H_s = H_s^G - H_s^r$, then

$$\Delta A_s = -\sigma_x^{-2}[(\Delta R_s)\mathbf{P}_s^G + R_s^r(\mathbf{P}_s^G - \mathbf{P}_s^B)],$$

$$\Delta D_s = \sigma_x^{-1}[(\Delta R_s)\mathbf{P}_X^{B*}(\mathbf{X}_s) + R_s^r(\mathbf{P}_X^{B*}(\mathbf{X}_s^G) - \mathbf{P}_X^{B*}(\mathbf{X}_s))],$$

are both of order ε in L_C^{2q} by part (i). Likewise $\Delta C_s = -(\Delta A_s)\mathbf{U}_t^B$ is of order ε in L^q by part (i). Moreover $\mathbf{U}_t^g$ is the solution to the following:

$$d\mathbf{U}_t^g = (-\Gamma^g + i\Omega_\varepsilon)\mathbf{U}_t^g dt + F_t^g dt + \Sigma_u^g dW_u^g(t),$$

and the differential of each column of B_t^{r*} can be written as

$$d[B_t^{r*}]_{\mathbf{K}_g,\mathbf{k}} = \sigma_x^2 d[Q_t^* R_t^{r*}]_{\mathbf{K}_g,\mathbf{k}} = b_t dt + \Sigma_t dW_t^x$$

with $|b_t| \leq b(|\mathbf{U}_t^g| + |\mathbf{U}_t^B| + 1), \|\Sigma_t\| \leq b$ for an ε-uniform b, (this b could depend on $\vec{v}_{t\geq 0}^B$). From here, the proof follows exactly the same as the one of Theorem 3.3 after the line of (4.4); the only difference is m_t^g is replaced by $\mathbf{U}_t^g$, $\mathbb{P}$ replaced by $\mathbb{P}_{\vec{v}^B}$. $\qquad\square$

5 Numerical experiments for filtering performance

The exact analytic expressions for the filter statistics for the two optimal filters and the reduced filter enable us to perform numerical experiments without further approximation. Our goals here are to assess filter performance both for small ε as well as moderate ε. Here are the details of our setups.

Recall the random rotating shallow water flow (2.1) and the evolution of the corresponding random amplitudes (2.2) described in Section 2. We set $d_B = d_g = 0.05$ in (2.2) such that the decorrelation time for both the GB and gravity modes is around 20. The parameter δ in (2.3) is set to be 1, implying that the values of Rossby and Froude number are the same. We consider the finite time interval $T \in [0, 40]$ and assume Fourier wavenumbers $\vec{k} = (k_1, k_2)$ in $[-2, 2]^2$. Therefore, the total number of modes is $|\mathbf{K}| = 75$ with $|\mathbf{K}_B| = 25$ GB modes and $|\mathbf{K}_g| = 50$ gravity modes. The GB modes of large scale $(0, 0)$, $(\pm 1, 0)$ and $(0, \pm 1)$ wavenumbers are deterministic while other GB modes and all gravity modes are stochastic. One reason to regard the leading GB modes to be deterministic is because people usually have some knowledge about the large scale motion in practice. Uniform energy spectrum is utilized for the stochastic modes in different wavenumbers with $E_{\mathbf{k}} = \sigma_{\vec{k},0}^2/(2d_B) = 3/10$ in each GB mode and $E_{\mathbf{k}} = \sigma_{\vec{k},\pm}^2/(2d_g) = 1/10$ in each gravity mode, respectively.

The deterministic forcing $f_{\vec{k},0}$ and $f_{\vec{k},\pm}$ in (2.2) have the following form

$$f_{\vec{k},0} = a_{\vec{k},0} \cos(\phi t) + b_{\vec{k},0}, \qquad \text{for } \vec{k} = \vec{0},$$
$$f_{\vec{k},0} = a_{\vec{k},0} \exp(\mathrm{i}\phi t) + b_{\vec{k},0}, \qquad \text{for } \vec{k} \neq \vec{0},$$

and

$$f_{\vec{k},\pm} = a_{\vec{k},\pm} \exp(\mathrm{i}\phi t) + b_{\vec{k},\pm}, \qquad \text{for all } \vec{k}.$$

Here, we pick up $b_{\vec{k},0} = \sqrt{3}/20$ for mode $\vec{k} = (0, 0)$, $b_{\vec{k},0} = \sqrt{3}/20(1 + \mathrm{i})$ for modes $(1, 0)$ and $(0, 1)$ and $b_{\vec{k},0} = \sqrt{3}/20(1 - \mathrm{i})$ for modes $(-1, 0)$ and $(0, -1)$. The mean forcing $b_{\vec{k},0}$ and $b_{\vec{k},\pm}$ for the stochastic modes are all set to be zero. Besides, we set $a_{\vec{k},0} = \sqrt{3}/10$ and $a_{\vec{k},\pm} = 1/10$ for all $\vec{k}$ and therefore the amplitude of deterministic forcing is slightly larger than that of the stochastic forcing. Finally, we take $\phi = 2\pi/10$ such that the temporal period of the forcing is 10.

For the initialization of filters, the states of the GB mode in the largest scale $(0, 0)$ and all the stochastic modes are set to be consistent with the value at their statistical equilibrium. The initial values of the other four deterministic GB modes $(\pm 1, 0)$ and $(0, \pm 1)$, are all set to be zero, which is different from their equilibrium mean. The initial uncertainty of the stochastic modes is given by the equilibrium covariance of the dynamics (2.2) with $3/10$ and $1/10$ for each GB and gravity mode, respectively, while that of each deterministic GB mode is set to be $3/10$, which is the same as the equilibrium energy in all other stochastic GB modes. This initialization evidently satisfies Assumption 3.2.

The tracers used in the full filter (2.14)–(2.15) and the reduced filter (2.19)–(2.20) are identically the same, i.e., $\vec{X}_l(s)$ in (2.12). As shown in (2.12), the velocity of these tracers is the sum of the full velocity plus some noise. On the other hand, the tracers used in the GB filter (2.17)–(2.18) are $\vec{X}_l^B(s)$ in (2.13), which is based only on the GB part of the full flow and therefore are different from those in (2.12). For the sake of comparing the filtering skill, we impose the same observation noise process W_l^x in both (2.12) and

(2.13). Furthermore, the initial locations of the tracers used in both the full filter and GB filter are the same and are distributed uniformly in the periodic domain $\mathbb{T}^2 = [-\pi, \pi]^2$.

Two dynamical regimes will be considered. The first one is a fast rotation regime with small Rossby number $\varepsilon = 0.1$, which mimics motion in the midlatitude atmosphere or ocean [12]. Another dynamical regime involves moderate rotation with $\varepsilon = 1$. Note that the GB part of the flow is kept the same in both regimes and the only difference lies in the gravity part of the flow. We focus on the following issues:

- Recovery skill of the GB part of the flow using the full filter, and comparison with the idealized GB filter.

- The conditions that enable the imperfect filter, i.e. the reduced filter, to have high skill in filtering GB part of the flow.

- Uncertainty reduction in both GB and gravity parts of the flow using full filter.

The main results from numerics are summarized as follows with ε being the key parameter:

Comparison between the full and the GB filter

- Starting from the same location, the tracer trajectories of the two filters are close to each other in an order $O(1)$ time for $\varepsilon = 0.1$ as shown in Proposition 4.2 for $\varepsilon \ll 1$. The two trajectories depart quickly in the $\varepsilon = 1$ regime.

- The long-term averaged statistics in recovering the GB part of the flow using the full filter overlaps with that using GB filter in $\varepsilon = 0.1$ regime and is only slightly worse than the latter in $\varepsilon = 1$ regime. Filtering skill increases with the increase of L and decrease of σ_x.

- An information barrier [8] is observed with the increase of L using both filters in both regimes.

- The long-term distribution of the tracers' location using the full filter is nearly uniform in $\varepsilon = 0.1$ regime but highly non-uniform in the $\varepsilon = 1$ regime while that using the GB filter is always uniform due to the incompressibility.

Comparison between the full and the reduced filter

- The reduced filter is slightly worse than the full filter in filtering the GB part of the flow in the $\varepsilon = 0.1$ regime with moderate σ_x and L in agreement with Theorem 3.3; however, the reduced filter becomes quite inaccurate in $\varepsilon = 1$ regime.

- Different from the full filter, a smaller σ_x increases the error using the reduced filter in both regimes as anticipated by our theoretical comment, Remark 4.1.

- The initial error in the deterministic GB modes vanishes very quickly using the full filter in both regimes with a moderately large L. Using the reduced filter, the initial error goes down to some level quickly but a long time is required afterward for the error to reduce in the $\varepsilon = 1$ regime even with a large number of tracers L.

5.1 Comparison of filtering skill

To begin, we show the tracer trajectories of the full and GB filter within an order $O(1)$ time from $t = 0$ to $t = 3$ in Figure 5.1. Although the trajectories illustrated in this figure are from a simulation with 10 tracers, only one tracer trajectory of each filter is shown for the conciseness. Starting from the same location, the two trajectories almost overlap with each other when $\varepsilon = 0.1$ with both small and large observation noise σ_x as shown in top panels. On the other hand, when ε increases to 1, the two trajectories diverge very quickly, which is shown in the bottom panels. This is consistent with Proposition 4.2.
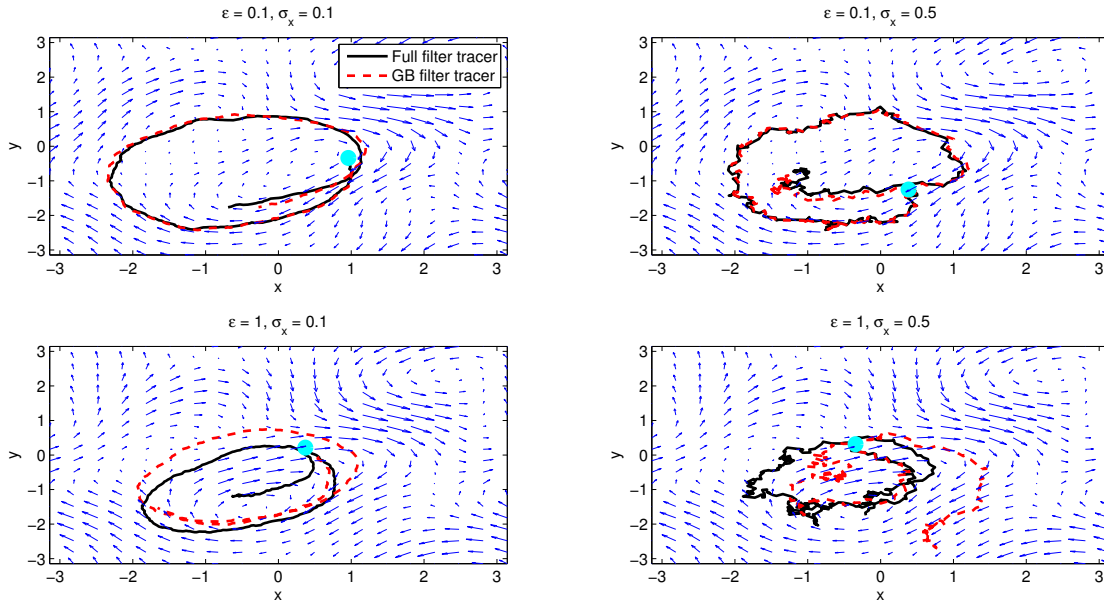
Figure 5.1: Comparison of one tracer trajectory of the full filter (solid) and one of the GB filter (dashed) starting from the same location from $t = 0$ to $t = 3$ with different ε and σ_x. Both tracers are taken from the simulation with $L = 10$ but only one of the ten tracers is shown for each filter for conciseness. The background velocity field is the one at time $t = 3$. The initial location of both the tracers is the same and is denoted by a cyan solid circle.

In the following, we compare the filtering skill in recovering the GB part of the flow using the three filters. Since the recovered GB flows are incompressible, we plot their steamlines in Figure 5.2 at time $t = 15$ with $L = 20$ and $\sigma_x = 0.2$. Notably, in the $\varepsilon = 0.1$ regime, the recovered streamlines using the three filters are all close to the truth with slight differences around the two vortices in the center. However, for the $\varepsilon = 1$ regime, the recovered streamlines using the reduced filter have a large difference compared with the truth in both the vortices in the center and the flow in the right top and bottom parts of the panel while the full and GB filters retain high filtering skill.

Other than visual figures, the phenomena mentioned above can also be measured through statistical quantities. The root-mean-L^2-error made by the recovered flow at a fixed time t is given by:

$$\text{root-mean-}L^2\text{-error} = \sqrt{\frac{1}{|\mathbb{T}^2|} \int_{\mathbb{T}^2} \left| \vec{v}_*(\vec{x}, t) - \vec{v}_f(\vec{x}, t) \right|^2 d\vec{x}},$$
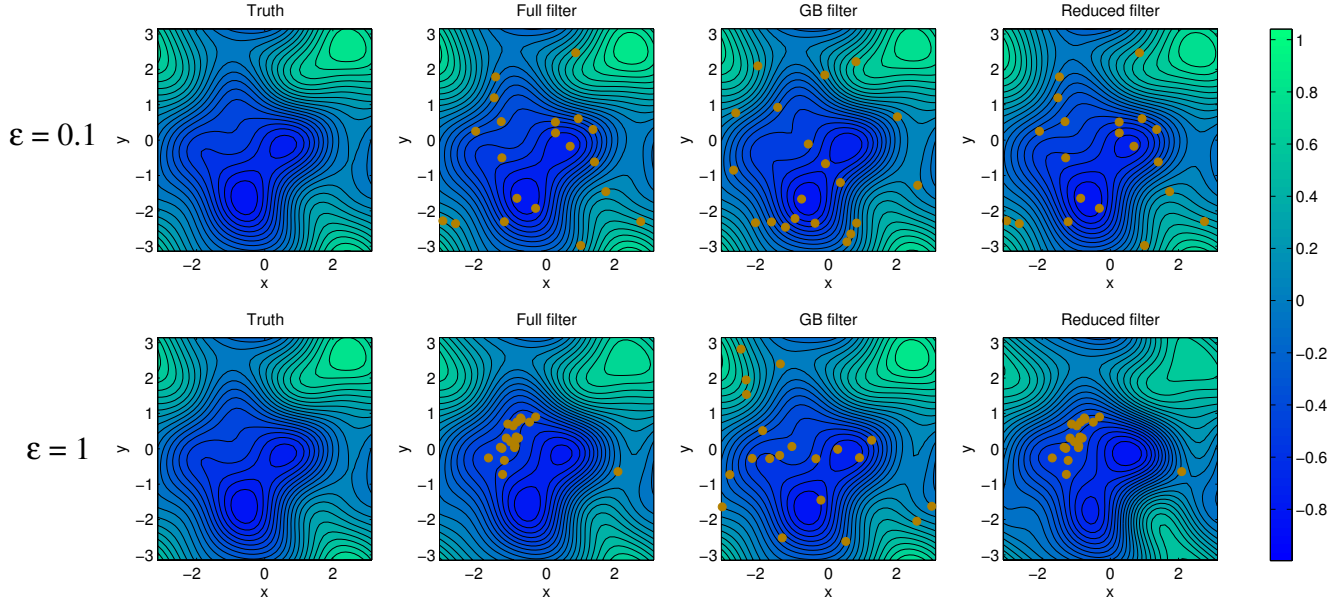
23

Figure 5.2: Recovered streamlines regarding only the GB part of the flow at $t = 15$ with observation noise $\sigma_x = 0.2$ and the number of tracers $L = 20$. Here the Rossby number $\varepsilon = 0.1$ for the top panels and $\varepsilon = 1$ for the bottom ones. The first column shows the streamlines of the truth and the other three columns show the recovered streamlines using full filter, GB filter and reduced filter, respectively. The circles represent the location of the tracers at current time.

where $\vec{v}_*$ and $\vec{v}_f$ are the true and filtered two-dimensional velocity field and $\mathbb{T}^2 = [-\pi, \pi]^2$ with $|\mathbb{T}^2|$ denoting its area. Figure 5.3 illustrates the root-mean-L^2-error of the recovered streamlines of GB flow comparing with the truth for all the three filters as a function of L at three different times. The middle column shows the filtering skill at $t = 15$, corresponding to Figure 5.2. Notably, for $\varepsilon = 0.1$ the reduced filter has a precision slightly worse than the perfect filter but within a satisfactory range; for $\varepsilon = 1$ the gap between the reduced filter and the full filter increases enormously. Similar phenomenon exists for $t = 30$, longer than decorrelation time $\tau_{corr} = 20$, indicating this is a persisting behavior. By comparing with the $t = 1$ column, it is inferred that this gap between the reduced and full filter likely grows with time and eventually reaches an equilibrium level [23] . On the other hand, the filtering skill using the full filter in $\varepsilon = 0.1$ regime is almost exactly the same as that using GB filter and is only slightly worse than the latter in $\varepsilon = 1$ regime. All these observations are consistent with Theorems 3.3 and 3.4, which state that the error gap between the filters decreases with ε.

To study the underlying reason for the behavior discussed above, it is necessary to look at the posterior mean estimation of the Fourier coefficients for the GB part using different filters. Since the energy is assigned in an equipartition way, all the modes have similar behavior. In the following, wavenumber $(2, 2)$ is picked to illustrate phenomena that are generally true for other wavenumbers. The posterior mean estimation of wavenumber $(2, 2)$ is shown in Figure 5.4. The recovered Fourier coefficients using both full filter and GB filter are close to the truth as long as L is not too small. Regarding the estimation using reduced filter, in $\varepsilon = 0.1$ regime most of the gravity waves are smoothed out with the increase of L. The recovered GB mode approaches the truth with only small

oscillation using more than $L = 20$ tracers; see the enlarged graph inside the top right panel. However, the situation deteriorates severely with an order one Rossby number. A significant amplitude of oscillation around the true value is observed using the reduced filter even with $L = 200$ tracers, which leads to the large error.

The next step is to investigate the dependence of the reduced filter in two key observation parameters: L and σ_x. Recall that one standard measurement of filtering skill is the root-mean-squared (RMS) error between the true signal $\mathbf{U}_t$ and the maximum likelihood filter estimate $\vec{m}_t$,

$$\mathrm{RMSE} = \sqrt{\tfrac{1}{T} \int_0^T |\vec{m}_s - \mathbf{U}_s|^2 \mathrm{d}s}. \tag{5.1}$$

Below, $\mathbf{U}_s$ and $\vec{m}_s$ are the truth and posterior mean estimation of the Fourier coefficient of wavenumber $(2, 2)$ and $T = 40$. The left column of Figure 5.5 shows the RMS error in the posterior mean estimation for GB mode. For the optimal filters, full filter and GB filter, the RMS errors decay with L and the decay rate becomes slower when L becomes large. The reduced filter is slightly inferior to its counterparts in the small ε regime but much worse in order one ε regime. These observations are consistent with those in Figure 5.2 and 5.3.

The dependence of the RMS error on the observation noise σ_x is shown in Figure 5.6. Here, one particularly interesting phenomenon arises: while the optimal filters, full and GB filter, perform better with smaller σ_x, the error made by the reduced filter grows. This intriguing plot can be explained as follow: A small observation noise enforces the posterior state to put more trust towards the observation. Yet, the observation of the reduced filter contains both GB and gravity parts of the flow while the dynamics involves only the GB part. Therefore, the reduced filter regards the superposition of GB and gravity parts as the filtered GB part and results in a large error, especially with larger ε.

In the previous figures, the performance of the full filter is similar to the GB filter. Yet if we align Figures 5.3-5.6, the following two patterns hold among all filtering criterion, which are in accordance with Theorem 3.4:

- When $\varepsilon = 0.1$, the statistics of both the full and the GB filter almost collapse with each other;

- When $\varepsilon = 1$, there is an observable difference between the two filters. The GB filter recovers the GB flow better, as its observations are not corrupted by the gravity waves.

It is worth mentioning that, according to our previous results in [8] for incompressible flow, we have explicit characterizations of the GB filter's behavior for large L. Based on the finding from the previous figures, these characterizations work perfectly for the full filter when ε is small, and provide good reference when ε is of order one.

To understand how the gravity waves interfere with the full filter, the true and recovered full velocity field at $t = 15$ with different number of tracers L are shown in Figure 5.7. The dots on top of the recovered velocity field indicate the current locations of the tracers. In both regimes, two tracers are already sufficient to capture the rough profile of the velocity field. Yet, evident errors are observed from the recovered velocity field which diminishes with the increase of L. From this figure, it is also obvious that the distribution of the tracers is nearly uniform in the small Rossby number regime while being highly non-uniform in $\varepsilon = 1$ regime. Using Theorem 3.1 of [8] and the Fokker Plank equation

for each tracer given $\vec{v}_{s\geq0}$, we know the uniform distribution is the invariant distribution for the tracers if and only if the underlying flow is incompressible. Together with Proposition 4.2, our result indicates that fast rotation leads to a nearly uniform distribution of the tracers, due to the fast averaging effects of the gravity waves on the trajectories. Following the proof of [8], the configuration of the tracers actually plays a decisive role in the filters' behavior. Hence it is very likely that the similarity of the full filter with the GB filter is caused by the approximately uniform distribution of tracers in the fast rotating regime. On the other hand, as shown in Figures 5.2 and 5.7, for $\varepsilon = 1$ the effect of compressibility on the Lagrangian trajectories is substantial leading to pronounced clustering of these trajectories.
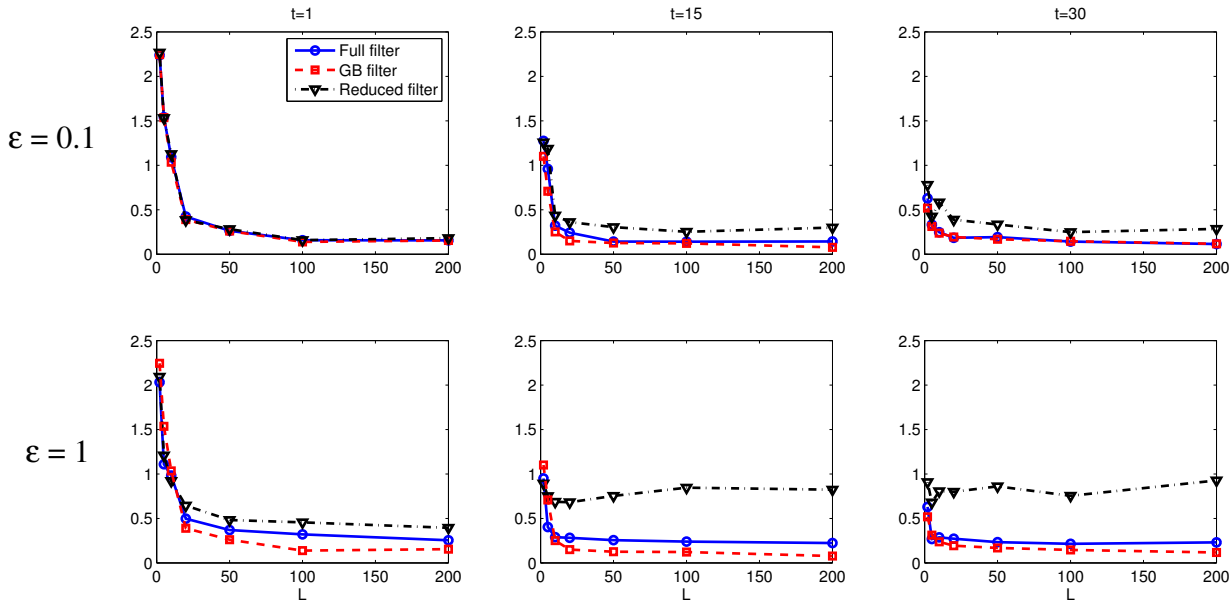
Figure 5.3: Root-mean-L^2-error in the recovered GB part of the velocity field comparing with the truth as a function of the number of tracers L. The observation noise $\sigma_x = 0.2$ is fixed. Top and bottom panels are for the case with $\varepsilon = 0.1$ and $\varepsilon = 1$, respectively. Left column shows the skill using full filter (circle), GB filter (rectangle) and reduced filter (triangle) at time $t = 1$ and the middle and right columns show that at time $t = 15$ and 30, respectively, where the decorrelation time of the system is $\tau_{corr} = 20$.

Finally, we study filtering with initial uncertainty of the large scale deterministic GB modes $(\pm1, 0)$ and $(0, \pm1)$. Note that the GB mode $(0, 0)$ cannot be filtered because the first two components of the associated eigenvector (2.5) are zero, meaning that there's no observablility of the mode [21]. Recall that the initial values for these four deterministic GB modes $(\pm1, 0)$ and $(0, \pm1)$ are set to be zero, which are different from the values at the equilibrium. In addition, an initial uncertainty, which equals the equilibrium energy of the other GB modes, is assigned for each of these modes.

Figure 5.8 shows the evolution of posterior mean of GB mode $(1, 0)$ as a function of time with different number of tracers L. It is no surprise that increasing L accelerates the convergence of the posterior mean estimation to the equilibrium value. With $L = 2$, the posterior mean estimation of the full filter still has a large gap compared with the equilibrium value while that gap is almost negligible using more than 10 tracers. This again explains the improvement of the recovered velocity field with L in Figure 5.7.
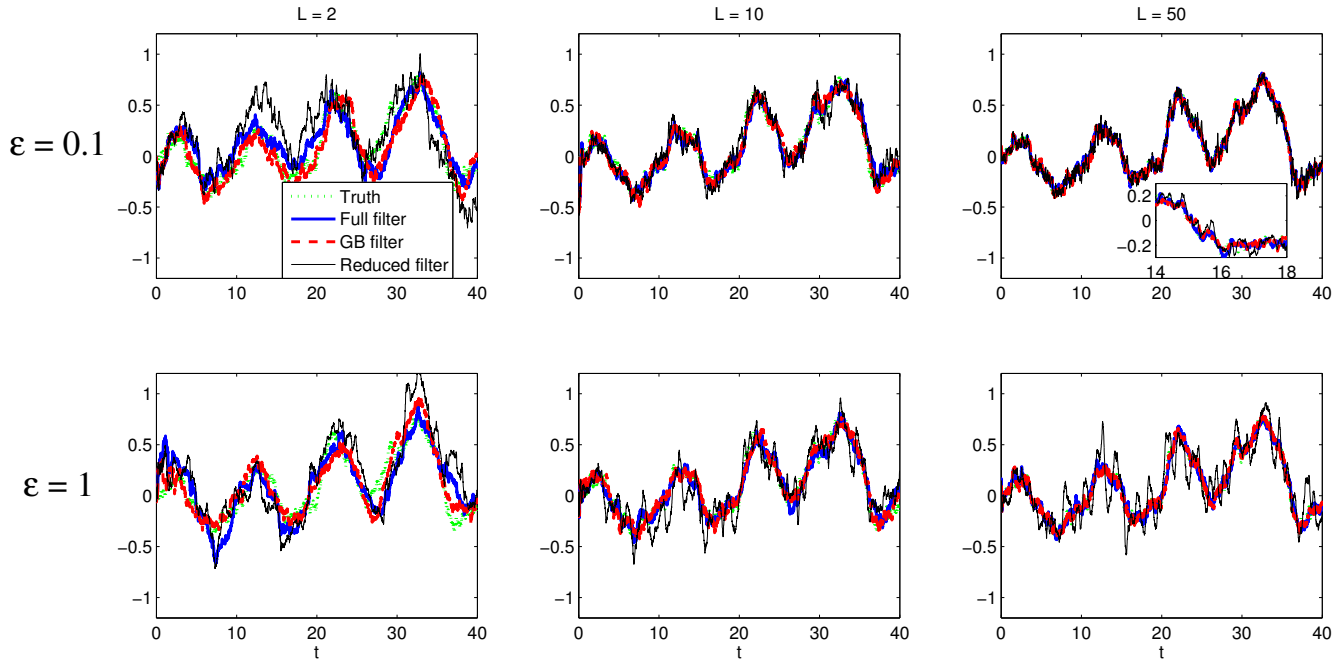
Figure 5.4: Comparison of the posterior mean estimation for the GB mode of wavenumber $(2, 2)$ as a function of time with different filters. Here, the observation noise is $\sigma_x = 0.2$. The dotted green curve shows the true realization. The blue solid curve, red dashed curve and thin black solid curve show the posterior mean estimation of full filter, GB filter and reduced filter, respectively.

Also, the mean estimation with filtering converges more quickly than the unfiltered one. However, when ε is of order one, it takes a long time for the posterior mean of the reduced filter to converge even with $L = 50$. This is because with a large number of tracers the posterior mean estimation approaches the observation very quickly and the posterior covariance goes down to zero very quickly. However, because the gravity modes are involved in the observation, the posterior mean estimation of this process contains some error. Yet, due to the quick reduction of the covariance, the filter estimation trusts the dynamics more afterwards and thus a long time is required for convergence because of the dynamics' weak damping.

Our other numerical experiments, which are not shown here, indicate that a small observation noise helps accelerate the convergence of the filter estimation when the initial value is far from the equilibrium. Yet, similar pathological phenomena are observed for the reduced filter in $\varepsilon = 1$ regime; although the small observation noise pulls its estimation to a near equilibrium state very quickly, it takes a long time for the posterior mean to converge afterwards. Another conclusion is that starting from a non-equilibrium state a large initial uncertainty actually helps both the full and GB filters converge, because a large initial uncertainty implies the filter trusts the observations more quickly.
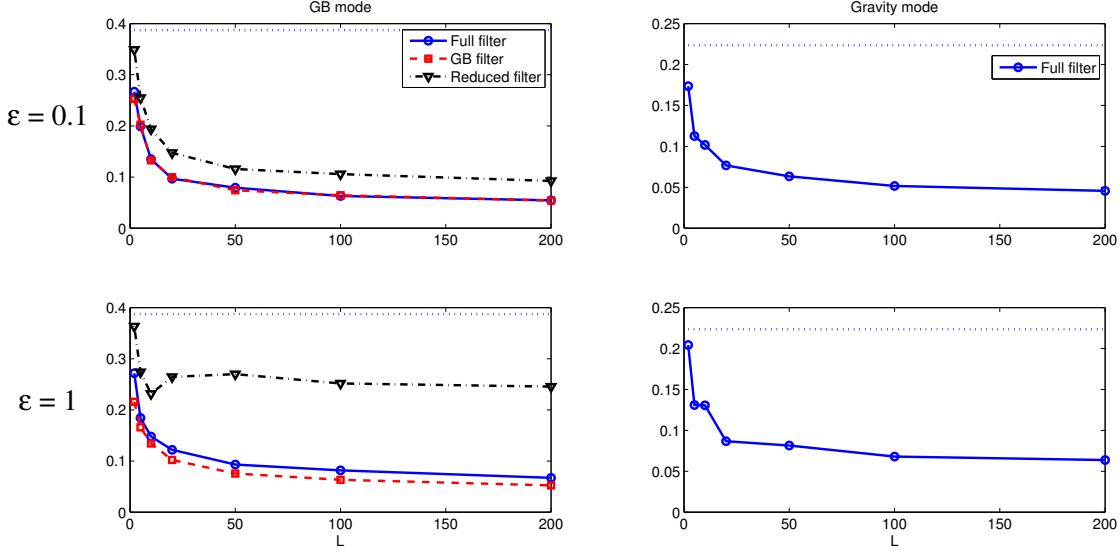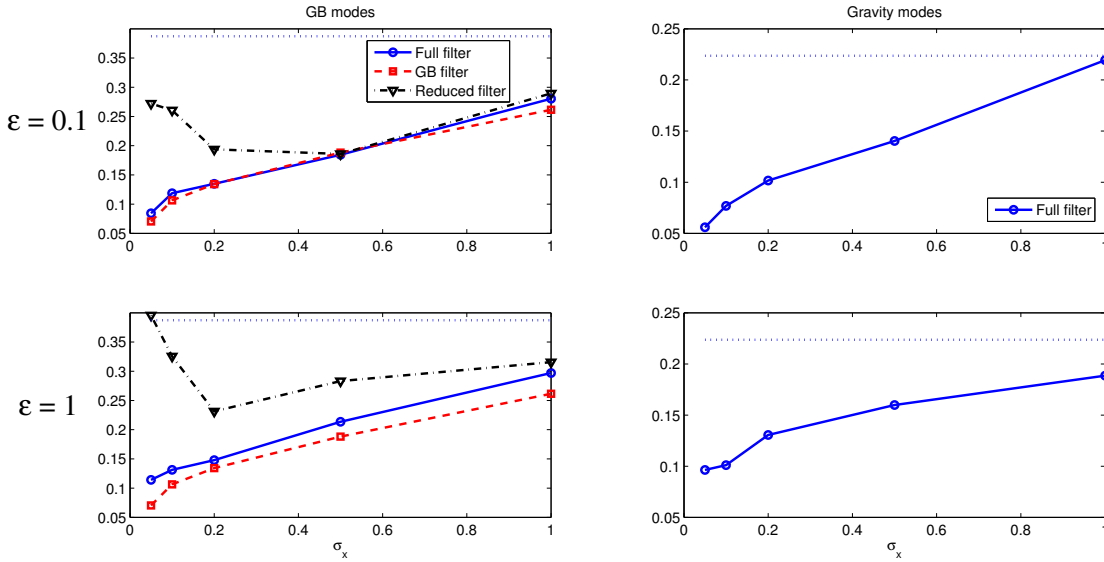
Figure 5.5: RMS error across time $t \in [0, 40]$ in the posterior mean comparing with the true signal as a function of the number of tracers L for wavenumber $(2, 2)$. The observation noise $\sigma_x = 0.2$ is fixed. Top and bottom panels show the case with $\varepsilon = 0.1$ and $\varepsilon = 1$, respectively. Left panels show the skill in the GB mode for full filter (circle), GB filter (rectangle) and reduced filter (triangle) and the right panels show that in the gravity mode for the full filter. The blue dotted lines show one standard deviation of the equilibrium distribution without filtering.

Figure 5.6: RMS error across time $t \in [0, 40]$ in the posterior mean comparing with the true signal as a function of the observation noise σ_x for wavenumber $(2, 2)$. The number of tracers $L = 10$ is fixed. Top and bottom panels are for the case with $\varepsilon = 0.1$ and $\varepsilon = 1$, respectively. Left panels show the skill in the GB mode for full filter (circle), GB filter (rectangle) and reduced filter (triangle) and the right panels show that in the gravity mode for the full filter. The blue dotted lines show one standard deviation of the equilibrium distribution without filter.
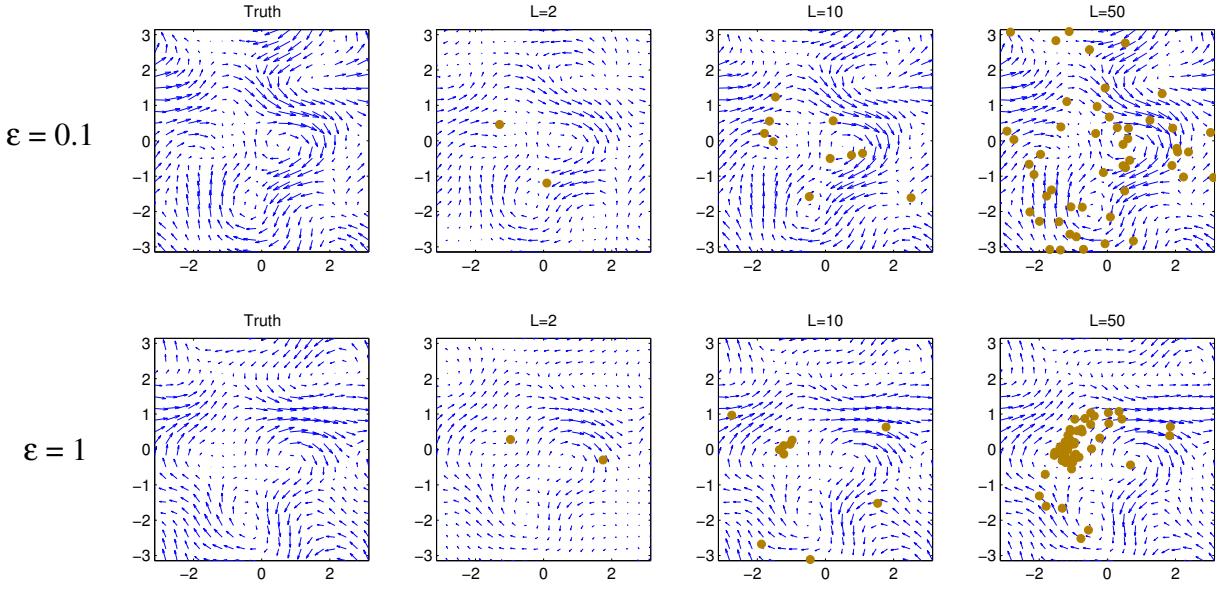
Figure 5.7: Full velocity field recovered from full filter with observation noise $\sigma_x = 0.2$ at time $t = 15$. Here the Rossby number $\varepsilon = 0.1$ for the top panels and $\varepsilon = 1$ for the bottom ones. The first column shows the true velocity field and the other three columns show the recovered velocity field with 2, 10 and 50 tracers, respectively. The circles represent the location of the tracers at current time.
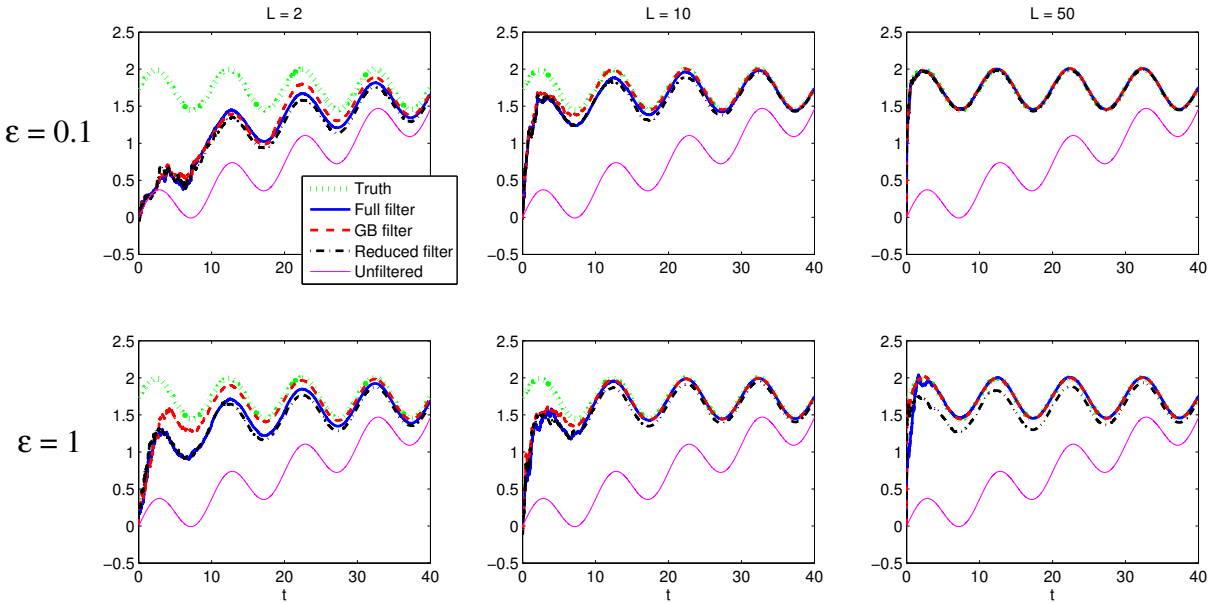

Figure 5.8: Posterior mean of the deterministic mode $(1, 0)$ with different number of tracers L and Rossby number ε as a function of time. The observation noise $\sigma_x = 0.2$ is fixed. The initial value of prior mean is zero, which is not the equilibrium state, and an initial uncertainty is imposed.

5.2 Uncertainty reduction in rotating compressible flows

Another important quantity that characterizes the performance of filters is the uncertainty reduction, computed by (2.21):

$$\mathcal{P}(p,q) = \left[\tfrac{1}{2}(\vec{m}_p - \vec{m}_q)^T R_q^{-1}(\vec{m}_p - \vec{m}_q)\right] + \tfrac{1}{2}\left[\text{tr}(R_p R_q^{-1}) - N - \ln\det(R_p R_q^{-1})\right],$$

where the terms in the first and second bracket are the signal and dispersion part, respectively. Figures 5.9 and 5.10 show the averaged uncertainty reduction across time in all stochastic GB modes and all gravity modes as a function of L. Rigorously speaking, the application of (2.21) to the reduced filter is at most formal since this filter is non-optimal [23]; we plot it to have better understanding of the reduced filter. By applying Corollary 3.4 of [8] to the uncertainty in GB modes from GB filter, it is known when $L \to \infty$:

- The signal part converges to a limit value computed by replacing the posterior mean by the truth in the signal part of (2.21);

- The dispersion part grows as a logarithmic function of L, forming an information barrier in practice.

In Figure 5.9, the plots of the full filter overlap with those of the GB filter in the $\varepsilon = 0.1$ regime in both signal and dispersion parts; for $\varepsilon = 1$, the full filter reduces about 30% less uncertainty in the dispersion part while matching the performance of the GB filter in the signal part. This indicates the uncertainty reduction criterion given by [8] works very well for fast or slow rotational compressible random flows. The anomalously high uncertainty reduction of the reduced filter in the signal part for $\varepsilon = 1$ actually indicates its erroneous performance: the oscillating error it makes in posterior mean contributes greatly in the computation of the signal part. Figure 5.10 indicates the uncertainty reduction made by the full filter in the gravity modes is similar to the GB modes, and more uncertainty is reduced in the small ε regime than order one ε regime.

Likewise, the dependence of the uncertainty reduction on the observation noise σ_x is shown in Figure 5.11. The averaged uncertainty reduction in the dispersion part has an obvious decay in both GB and gravity modes due to the increase of the observation noise. Again, the behavior of GB filter gives a perfect reference for the full filter when $\varepsilon = 0.1$ and gives a satisfactory reference for $\varepsilon = 1$. It is worth mentioning that the reduced filter produces anomalously high uncertainty reduction in the signal part for small σ_x (not shown here). Recalling Figure 5.6, we know in the small σ_x scenario the reduced filter relies too much on the observations, which perturbs its estimation of the GB modes.
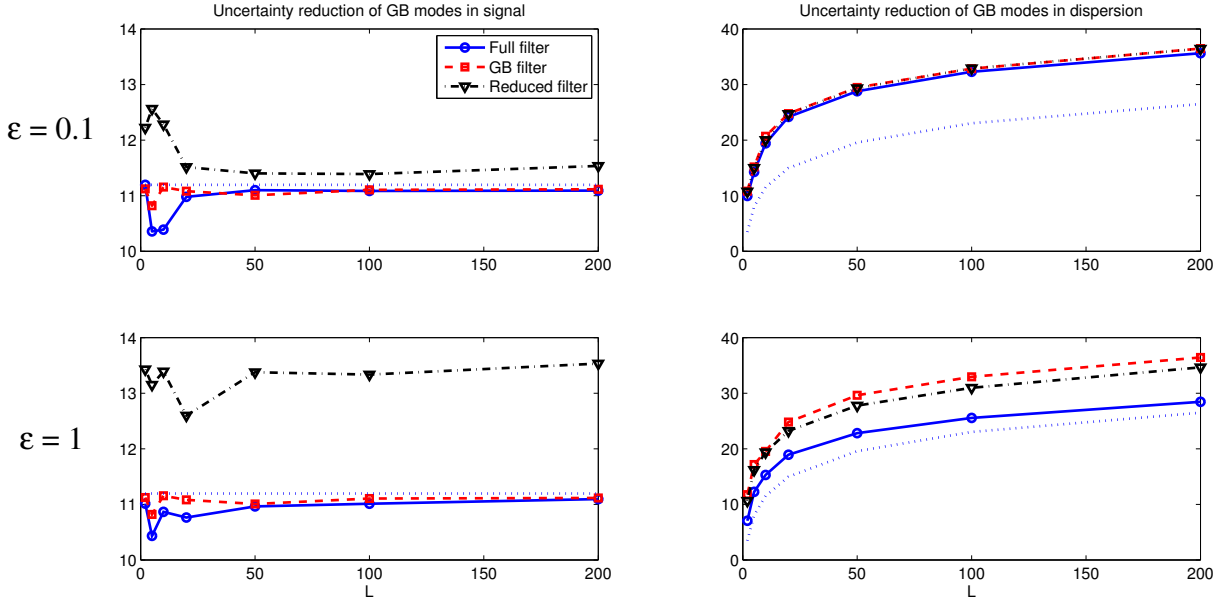
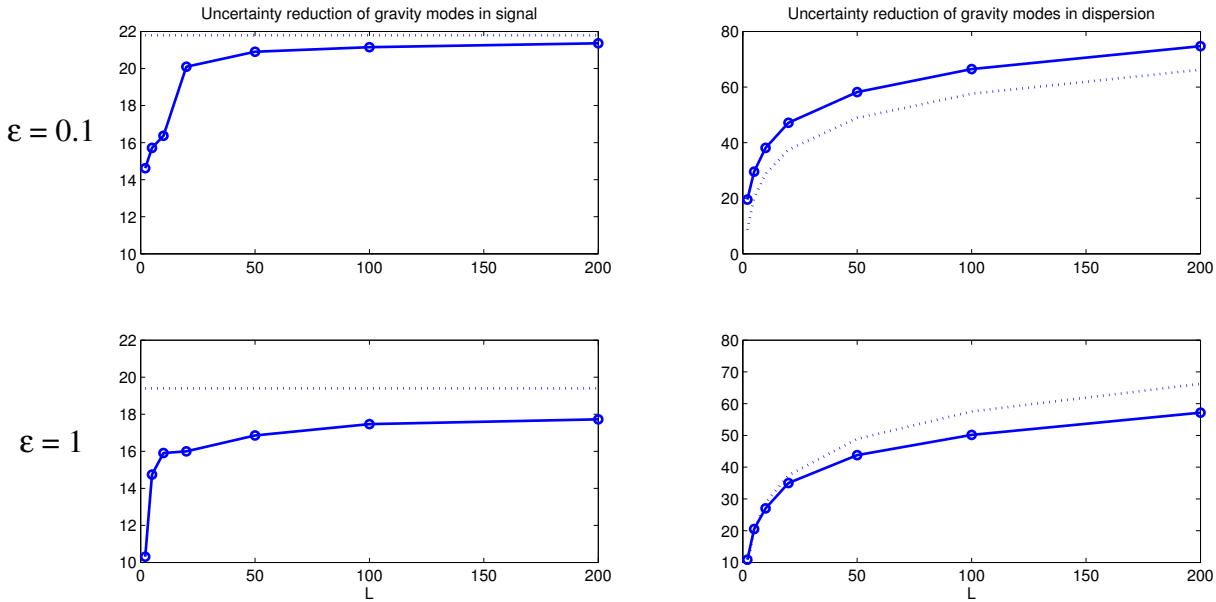Figure 5.9: Averaged uncertainty reduction across time $T \in [0, 40]$ in all the GB modes as a function of the number of tracers L for full filter (circle), GB filter (rectangle) and reduced filter (triangle). The observation noise $\sigma_x = 0.2$ is fixed. Top and bottom panels are for the case with $\varepsilon = 0.1$ and $\varepsilon = 1$, respectively. Left panel shows the uncertainty reduction in signal, where the blue dotted line indicates the limit value of uncertainty reduction for the full filter as $L \to \infty$. Right panel shows the uncertainty reduction in the dispersion part, where the blue dotted curve indicates the growth rate of $\ln(L)$.

Figure 5.10: Averaged uncertainty reduction across time $T \in [0, 40]$ in all the gravity modes as a function of the number of tracers L using full filter. Same illustrations as those in Figure 5.9.
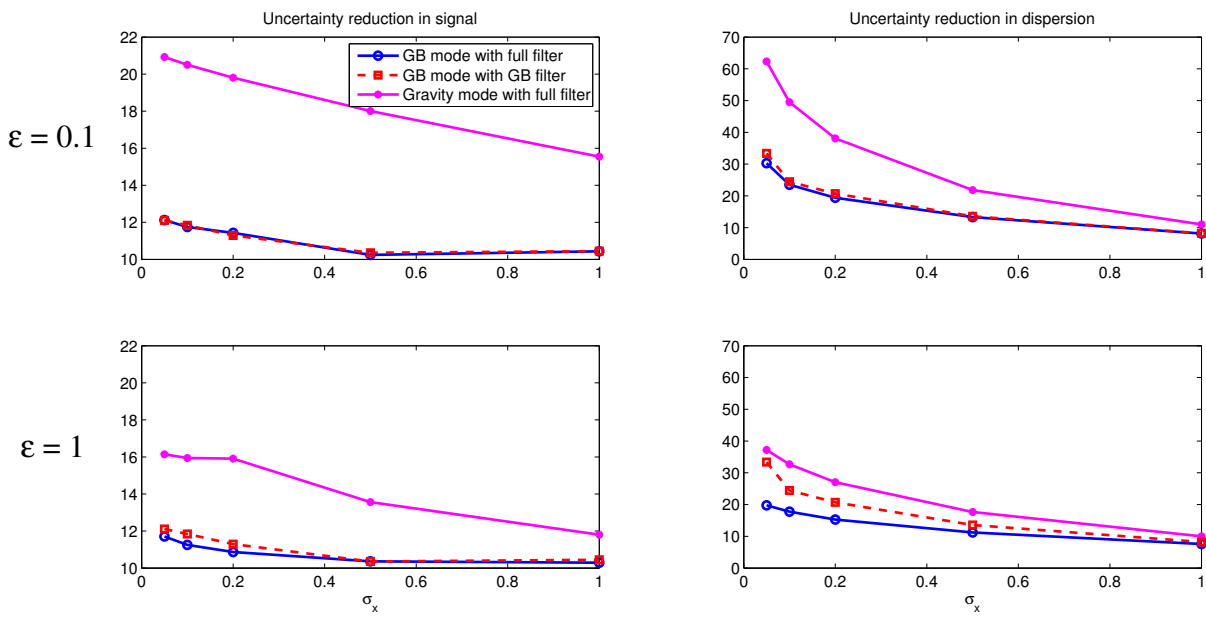
31

Figure 5.11: Averaged uncertainty reduction across time $T \in [0, 40]$ in all the GB modes as a function of the observation noise σ_x. The number of tracers $L = 10$ is fixed. Top and bottom panels show the case with $\varepsilon = 0.1$ and $\varepsilon = 1$, respectively. Left panel shows the uncertainty reduction in signal and right panel shows the uncertainty reduction in the dispersion part.

6 Conclusions and Discussion

In this paper, the impact of the gravity waves over the filtering skill of L noisy Lagrangian tracers is investigated from two angles. The recovery of a random flow with both geostrophically balanced (GB) part and gravity waves is theoretically represented by a full filter derived from conditional Gaussian theory [9]. The full filter is then compared with a reference GB filter, which is clean without gravity waves and by [8] we have clear knowledge. The second angle comes from the practical need of imperfect filters, as most often the GB flows are the only part of concern and have resolved dynamics, while the tracers are transported by the gravity waves as well. This aim is achieved by applying the GB filter's formulas to tracers transported by both parts of the flow field, forming the reduced filter. The key finding of the current work is that the three filters produce results close to each other as long as the Rossby number $\varepsilon \ll 1$.

As all three filters possess concrete analytical formulas derived from conditional Gaussian theory, asymptotic analysis for $\varepsilon \to 0$ can be applied to their difference. By exploiting the fast-wave averaging phenomenon of gravity waves, the key finding is proved with full mathematical rigor. The followup numerical simulations not only validate this result but also reveal that noisy Lagrangian tracers in fast rotational flows are distributed close to uniform and small observation error σ_x may force the reduced filter to rely too much on imperfect observations contaminated by the unresolved gravity waves. Consequently, the findings of this work imply that when $\varepsilon \ll 1$, the filtering of a rapidly rotating compressible flow has similar behavior as of its GB counterpart, and the geostrophic approximation is a good simplification strategy for imperfect filters.

Apart from these major conclusions, the following remarks are either implied by or related to our findings:

1. From a practical point of view, as the reduced filter has much simpler structure, heuristically its running speed is about $1/9$ of the full filter. Application of it is encouraged when only the GB part of the flow is of concern and ε is small. Moreover, the potential error induced is likely to have a obvious oscillating pattern, cf. Figure 5.4, and this is readily motivated.

2. According to the discussion in Section 5, the similarity between the full filter and the GB filter for $\varepsilon = 1$ may be caused by the distribution of the tracers being close to uniform. Actually, combining Proposition 4.2 and Theorem 3.1 of [8], we conjecture that the total variation distance between the distribution of $\vec{X}_l(s)$ and the uniform distribution is bounded by εM for a proper M as $s \to \infty$. This may shed light on understanding the long time Lagrangian filters' behavior in the fast rotating regime.

3. In contrast, it is also interesting to ask what would happen when the tracers are concentrated in a certain part of the region due to compressibility as illustrated for $\varepsilon = 1$ in Figures 5.2 and 5.7. Intuitively, more information should be recovered for the concentrated region. Using numerics with different initializations, [6, 7] sheds some light over this issue. Yet these results regarding local information have yet to be generalized into theory. Maybe the conditional Gaussian framework can be used to better understand these issues.

4. Since the GB part of the fast rotating filtering regime is close to that of a geostrophic system, by Theorem 3.3 (i) of [8], the posterior covariance is very likely to be close

33

to a deterministic matrix for large L. This implies an approximation for the reduced filter may be a candidate for even more efficiency: simply keep the deterministic matrix in Theorem 3.3 (i) of [8] as the posterior covariance and update only the posterior mean. This will save a lot of computational power for the high dimensional version of this problem. Such simplification strategy is generally known as 3DVAR.

5. Finally, we mention that all of the work presented here involves a prototype slow-fast system while the noisy Lagrangian tracers provide nonlinear observations which mix the slow and fast components [21]. Such multi-scale systems occur throughout science and engineering, and our results here are useful as prototype examples from that perspective.

References

[1] A Griffa, A D Kirwan, A J Mariano, T M Özgökmen, and Rossby T. *Lagrangian analysis and prediction of coastal and ocean dynamics.* Cambridge University Press, 2007.

[2] J Gould and et al. Argo profiling floats bring new era of in situ ocean observations. *Eos Trans. AGU*, 85(19):185–191, 2004.

[3] A Molcard, L I Piterbarg, A Griffa, T M Özgökmen, and A J Mariano. Assimilation of drifter observations for the reconstruction of the eulerian circulation field. *Journal of Geophysical Research: Oceans*, 108(C3):3056, 2003.

[4] L Kuznetsov, K Ide, and C K R T Jones. A method for assimilation of lagrangian data. *Mon. Wea. Rev.*, 131(10):2247–2260, 2003.

[5] A Apte, C K R T Jones, and A M Stuart. A bayesian approach to lagrangian data assimilation. *Dynamic Meteorology and Oceanography*, 60(2):336–347, 2008.

[6] H Salman, L Kuznetsov, C K R T Jones, and K Ide. A method for assimilating lagrangian data into a shallow-water-equation ocean model. *Mon. Wea. Rev.*, 134:1081–1101, 2006.

[7] H Salman, K Ide, and C K R T Jones. Using flow geometry for drifter deployment in lagrangian data assimilation. *Tellus A*, 60:321–335, 2008.

[8] N Chen, A J Majda, and X T Tong. Information barriers for noisy Lagrangian tracers in filtering random incompressible flows. *Nonlinearity*, 27:2133–2163, 2014.

[9] R S Liptser and A N Shiryaev. *Statistics of random processes. I, II,*, volume 5 of *Applications of Mathematics.* Springer-Verlag, 2001.

[10] C G Rossby. On the mutual adjustment of pressure and velocity distributions in certain simple current systems. *J. Marine Research*, 5(3-4):239–263, 1938.

[11] A E Gill. *Atmosphere-Ocean Dynamics*. Academic Press, 1982.

[12] A J Majda. *Introduction to PDEs and Waves for the Atmosphere and Ocean*, volume 9 of *Courant lecture notes*. American Mathematical Society, 2003.

[13] B Cushman-Roisin and J M Becker. *Introduction to Geophysical Fluid Dynamics*, volume 101. Academic Press, 2011.

[14] P F Embid and A J Majda. Averaging over fast gravity waves for geophysical flows with arbitrary potential vorticity. *Communications in Partial Differential Equations*, 21(3-4):619–658, 1996.

[15] A J Majda and P F Embid. Averaging over fast gravity waves for geophysical flows with unbalanced initial data. *Theoret. Comput. Fluid Dynamics*, 11:155–169, 1998.

[16] A J Majda. Challenges in climate science and contemporary applied mathematics. *Comm. Pure Appl. Math*, 65(7):920–948, 2012.

[17] A J Majda and M Branicki. Lessons in uncertainty quantification for turbulent dynamical system. *Discrete and Continuous Dynamical Systems*, 32(9):3133–3221, 2013.

[18] A J Majda and B Gershgorin. Link between statistical equilibrium fidelity and forecasting skill for complex systems with model error. *Proc. Natl. Acad. Sci.*, 108(31):12599–12604, 2011.

[19] M Branicki, N Chen, and A J Majda. Non-gaussian test models for prediction and state estimation with model errors. *Chin. Ann. Math.*, 34(1):29–64, 2013.

[20] J Pedlosky. *Geophysical Fluid Dynamics*. Springer-Verlag, 1987.

[21] A J Majda and J Harlim. *Filtering complex turbulent systems*. Cambridge University Press, Cambridge, UK, 2012.

[22] M Branicki and A J Majda. Quantifying uncertainty for predictions with model error in non-guassian systems with intermittency. *Nonlinearity*, 25(9):2543–2578, 2012.

[23] M Branicki and A J Majda. Quantifying filter performance for turbulent dynamical systems through information theory. *Comm. Math. Sci.*, to appear, 2014.

[24] R Kleeman. Measuring dynamical prediction utility using relative entropy. *J. Atmos. Sci.*, 59:2057–2072, 2002.

[25] A J Majda and X Wang. *Nonlinear Dynamics and Statistical Theories for Basic Geophysical Flows*. Cambridge University Press, Cambridge, UK, 2006.

[26] O Kallenberg. *Foundations of modern probability*. Probability and its Applications (New York). Springer-Verlag, 1997.

[27] N V Krylov. *Controlled Diffusion Processes*. Stochastic Modeling and Applied Probability. Springer-Verlag, 1980.

[28] P E Protter. *Stochastic Integration and Differential Equations*. Stochastic modeling and applied probability. Springer, 2005.

[29] H Abou-Kandil, G Freiling, V Ionescu, and G Jank. *Matrix Riccati Equations in Control and Systems Theory.* Systems & Control: Foundations & Applications. Birkhauser Verlag, 2003.

[30] M M Konstantinov and G B Pelova. Sensitivity of the solutions to differential matrix riccati equations. *IEEE trans. on automatic control*, 36(2):213–215, 1991.